J. Mt. Sci. (2025) 22(12): 4464-4489 e-mail: jms@imde.ac.cn http://jms.imde.ac.cn
https://doi.org/10.1007/s11629-025-9874-y

Original Article

Palaeoseismicity recorded in soft-sediment deformation structures within a 166-m-long drill core from Diexi Palaeolake, eastern Tibetan Plateau

LI Jingjuan[1,2] https://orcid.org/0000-0002-4133-1776; e-mail: fightingkhc@qq.com

JANSEN John D.[3*] https://orcid.org/0000-0002-0669-5101; e-mail: jdj@ig.cas.cz

CARLING Paul A.[4] https://orcid.org/0000-0002-8976-6429; e-mail: P.A.Carling@soton.ac.uk

ÇINER Attila[5] https://orcid.org/0000-0002-6755-8426; e-mail: cinert@itu.edu.tr

FAN Xuanmei[2*] https://orcid.org/0000-0003-1049-6356; e-mail: fxm_cdut@qq.com

**Corresponding authors*

1 Chengdu Center of China Geological Survey (Geosciences Innovation Center of Southwest China), Chengdu 610081, China

2 State Key Laboratory of Geohazard Prevention and Geoenvironment Protection, Chengdu University of Technology, Chengdu 610059, China

3 GFÚ Institute of Geophysics, Czech Academy of Sciences, Prague 14131, Czechia

4 Geography & Environmental Science, University of Southampton, Southampton SO17 1BJ, UK

5 Eurasia Institute of Earth Sciences, İstanbul Technical University, Maslak-İstanbul 34398, Türkiye

Citation: Li JJ, Jansen JD, Carling PA, et al. (2025) Palaeoseismicity recorded in soft-sediment deformation structures within a 166-m-long drill core from Diexi Palaeolake, eastern Tibetan Plateau. Journal of Mountain Science 22(12). https://doi.org/10.1007/s11629-025-9874-y

Abstract: Soft-sediment deformation structures (SSDS) in water-saturated, unconsolidated sediments are the product of various causes and provide a valuable record of environmental and geological perturbations. We report a record of SSDS preserved in a ~166 m-long drill core (DX-2) extracted from the Late Pleistocene Diexi Palaeolake, eastern Tibetan Plateau. Two factors make this an outstanding site for studying SSDS: (1) it is among the most seismically active regions on Earth, and (2) it has experienced extremely fast sedimentation rates (~15 mm/yr) thanks to the prodigious sediment supply from seismically perturbed hillslopes and rivers upstream. We describe and interpret 13 SSDS types within the DX-2 based on detailed sedimentological, morphological, and lithological analysis. We consider the genesis of the abundant SSDS observed in the DX-2 core with several possibilities: mass movement, rock avalanche-driven tsunamis, rapid sedimentation, and seismic shaking as the most probable triggering mechanisms. We suggest high-intensity earthquakes of VI (Modified Mercalli Intensity) or greater as drivers of SSDS in the DX-2. Based on our observations, we propose a conceptual model that attempts to explain the transition from ductile to brittle SSDS behaviour with progressive accumulation and consolidation of the sediment pile. This paper highlights the value of SSDS analysis in palaeo-earthquake identification, aiming to improve the applicability of SSDS as a palaeo-earthquake marker in alpine and canyon areas.

Keywords: Sedimentology; Sedimentation; Earthquake; DX-2 core

Received: 03-Jun-2025
1st Revision: 01-Aug-2025
2nd Revision: 11-Oct-2025
Accepted: 15-Nov-2025

1 Introduction

Soft-sediment deformation structures (SSDS) in water-saturated, unconsolidated sediments provide a

valuable record of environmental and geological perturbations through time. SSDS are attributed to a wide variety of causes that can be grouped into six main (non-exclusive) mechanisms: (1) gravity-induced loading and slumping (Monecke et al. 2004; Alsop and Marco 2013), (2) stream floods (Monecke et al. 2004; Gilli et al. 2013), (3) mass movements (Schnellmann et al. 2007; Kremer et al. 2015), (4) debris flows (Kiefer et al. 2021; Staley et al. 2021), (5) rapid sedimentation (Moretti et al. 2001), and (6) earthquakes. Of the five mechanisms, seismically-induced SSDS have received by far the greatest attention, typically with the aim of inverting seismic information from the SSDS record (Seilacher 1969; Obermeier 1996; Moretti and Sabato 2007; Pandey et al. 2009; Ettensohn et al. 2011; Owen et al. 2011; Ghosh et al. 2012; Moretti and Van Loon 2014; Zheng et al. 2015; Shanmugam 2016; Müller et al. 2021). In this regard, SSDS have been employed to (1) analyse the magnitude, intensity, depth, epicentre location, and direction to/from the source (Sims 1975; Allen 1986; Marco and Agnon 1995; Jones and Omoto 2000; Moretti 2000; Moretti et al. 2002; Neuwerth et al. 2006; Berra and Felletti 2011; Ghosh et al. 2012; Deev et al. 2019; Molenaar et al. 2024); (2) determine the recurrence intervals of seismicity and sedimentary responses (Sims 1973; Obermeier 1996; Calvo et al. 1998; Gibert et al. 2011; Moura-Lima et al. 2011; Rossetti et al. 2011; Wallace and Eyles 2015; Zheng et al. 2015); and (3) assess seismic risk (Suter et al. 2011; Gladkov et al. 2016; Deev et al. 2019).

Despite considerable research, identifying and discriminating the formation mechanisms of SSDS remain a major challenge given their differing tectonic, sedimentary, and lithological boundary conditions. Not least among these difficulties is that, as long as they exist in an unconsolidated state, SSDS are likely to experience multiple perturbations, resulting in broadscale overprinting of processes and forms (Agnon et al. 2006; Alsop and Marco 2011; Molenaar et al. 2019; 2021). This problem is especially marked in tectonically active mountain belts.

Two approaches characterise SSDS classifications: (1) the genetic approach, which attempts to identify the physical mechanisms that were active during the deformation (Neuwerth et al. 2006), and (2) the morphological, non-genetic approach, which accepts the limited knowledge of SSDS genesis and seeks to describe the structures in detail without attributing direct formative mechanisms. Attempts to combine these two approaches have also been proposed (e.g., Lowe 1975; Brenchley and Newall 1977; Allen 1982; Mills 1983; Owen 1987, 2003; Neuwerth et al. 2006). Much of the previous work identifying and classifying SSDS has been conducted on exposed sedimentary sections, which may provide a three-dimensional view of the structures (Montenat et al. 2007; Ettensohn et al. 2011; Qiao and Guo 2011; Rana et al. 2013; Wallace and Eyles 2015). Nevertheless, drill cores can offer much longer continuous vertical sequences, greatly multiplying the number of possible SSDS observations and facilitating the study of the entire active period of seismogenic faults (Koç Taşgın et al. 2011; Ezquerro et al. 2015; Zheng et al. 2015; Ezquerro et al. 2016; Törő and Pratt 2016). We apply genetic and morphological approaches here in our study of SSDS within a drill core from the Diexi Palaeolake in Sichuan, China.

Two factors make the Diexi Palaeolake an outstanding site for studying SSDS: (1) it is among the most seismically active regions on Earth, having experienced 18 earthquakes with $M \geq 6$ since 1930 (Chai and Liu 2002; Ma 2017), and (2) it is the locus of exceptionally rapid sedimentation rates (Wang et al. 2012). Here, we analyse SSDS within a ~166 m-long drill core (DX-2) extracted from the palaeolake. Based on a detailed sedimentological, morphological, and lithological analysis, we describe and interpret 13 SSDS types within DX-2. We then propose formative mechanisms to explain the SSDS, including how they may relate to the strong and frequent seismicity of the Diexi area.

2 Study Area

Diexi is located close to the eastern margin of the Tibetan Plateau within the upper reaches of the Minjiang River (Fig. 1). The Minjiang Valley is 60 to 300 m wide (Yang 2005; Jiang et al. 2016; Ma 2017; Zhang 2019) and is flanked by steep 30°–35° hillslopes with up to 3000 m of local relief (Zhang et al. 2011; Guo 2018). The largest dammed lake on the Minjiang River, Diexi Palaeolake, formed when a landslide (Fig. 1c) created a 400 m-high dam that blocked the valley at least 35 ka (Wang et al. 2020; Fan et al. 2021). The palaeolake measures ~26 km in length, 21.4 km^2 in area, and the total thickness of lacustrine sediments is ~370 m (Dai et al. 2023; Li et al. 2024). Sedimentation within the trough ended ~27 ka (Li et al. 2024) when the Minjiang River cut a new parallel epigenetic bedrock gorge (Fig. 1).

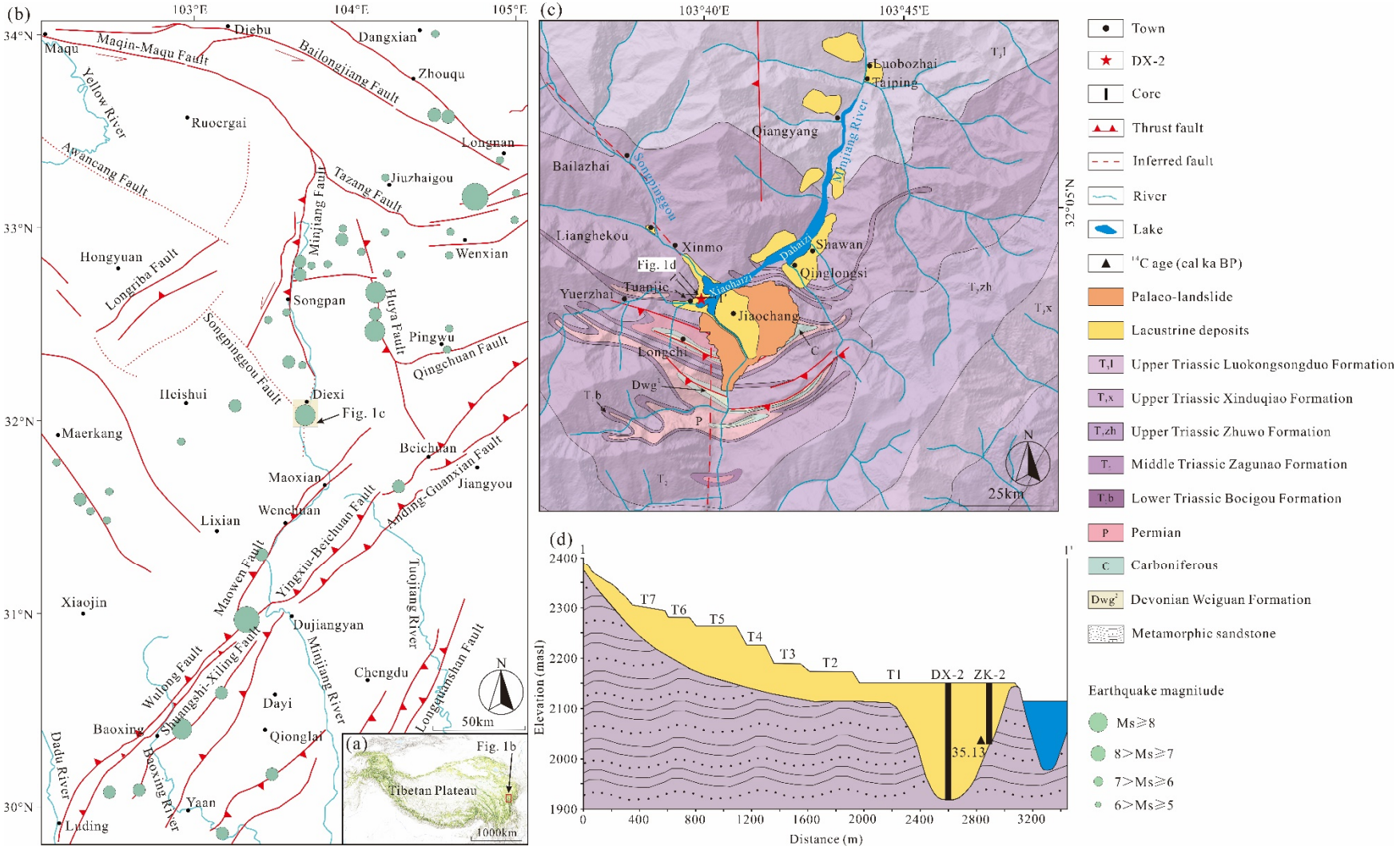

Fig. 1 Geological setting of the Diexi area and location of the DX-2 core: (a) Diexi relative to the Tibetan Plateau; (b) tectonic framework of the eastern Tibetan Plateau (Diexi is marked by yellow box); (c) generalised geological map of the Diexi area; (d) cross-section of the upper Minjiang valley showing cores DX-2 and ZK-2 (with basal age of 35.13 cal ka BP, Wang et al. 2012), and terraces T1 to T7 (maps modified from Zhang et al. 2016; Zhong et al. 2019; Wang et al. 2020; Fan et al. 2021).

The Tibetan Plateau and surrounding areas are subject to intense and frequent earthquakes linked to active tectonism (Yang et al. 1982; Chen and Lin 1993; Li and Fang 1998; Shi et al. 1999; Hou et al. 2001; Lu et al. 2004). The upper Minjiang River lies within the well-known 'north-south earthquake tectonic zone' (Tang et al. 1983; Huang et al. 2003; Yang 2005; Deng et al. 2013). Seismicity is primarily concentrated around the fault zones (Fig. 1b) (Shen 2014; Ren et al. 2018; Zhang 2019). The Diexi area is situated on the Minjiang Fault, a major south-to-north-trending thrust fault linked to at least six palaeoseismic events during the Holocene (Zhang et al. 2013; Li et al. 2018). Moreover, numerous other seismically active faults are located sufficiently close to cause notable shaking at Diexi (Fig. 1b, Table 1). Since 1930, the Diexi area has experienced thousands of earthquakes, including 57 events with M ≥ 4.7, among which 18 were of M ≥ 6 (Chai and Liu 2002; Ma 2017). Earthquakes are the primary cause of landslides (Wang et al. 2007; Gorum et al. 2011; Fan et al. 2017; Fan et al. 2018; Fan et al. 2019; Wu et al. 2019; Zhao et al. 2019; Dai et al. 2021), for example, at least 27 major landslides have been observed in the Diexi area: seven on the Songpinggou tributary (Fig. 1) and 20 on the Minjiang River (Zhao et al. 2019), including the giant landslide that formed Diexi Palaeolake (Wang et al. 2005; Wang et al. 2007; Wang et al. 2012; Fan et al. 2022) and the multiple devastating landslides caused by the 1933 Diexi earthquake (Chai et al. 1995; Dai et al. 2021). The frequent and voluminous sedimentary inputs have delivered high rates of sediment supply to the river channel network, which in turn produced extremely fast rates of sedimentation in Diexi Palaeolake, averaging ~15 mm/yr (Wang et al. 2012).

Between 40-30 ka, the regional palaeoclimate underwent three transitions from cold-dry to warm-humid conditions (Zhang et al. 2009), followed by more than ten alternations between cold and warm during 30-10 ka (Wang 2009; Wang et al. 2014).

Table 1 Active faults in the Diexi area and approximate recurrence activity according to previous studies

Faults	Characteristics	Active period	Palaeoseismic number (events)	Approx. recurrence interval#	References
Minjiang Fault	North-south thrust fault	10.23 ka–present	>6	<1705 yr	Zhang et al. (2013); Li et al. (2018)
Huya Fault	Northwest-trending right-lateral strike-slip fault	32.7 ka–present	–	–	Zhou et al. (2006)
Songpinggou Fault	Northwest-trending left-lateral thrust fault	20 ka–present	–	–	Tang et al. (1983); Ren et al. (2018); Zhao et al. (2023)
Wenmao Fault	Northeast-southwest right-lateral strike-slip reverse fault	50–20 ka	–	–	Deng et al. (1994); Zhou et al. (2006); Chen et al. (2007); Wang et al. (2017)
Qingchuan Fault	Northeast right-lateral strike-slip reverse fault	7.1–5.0 ka	>2	<4250 yr	Fan et al. (2008); Sun (2015)
Yingxiu-Beichuan Fault	Northeast-trending right-lateral strike-slip reverse fault	432 ka–present	Several times	–	Deng et al. (1994); Zhou et al. (2006); Chen et al. (2007)
Anding-Guanxian Fault	Northeast-trending reverse fault	14.3 ka–present	2	7150 yr	Deng et al. (1994); Chen et al. (2007)
Wulong Fault	Northeast-trending right-lateral strike-slip fault	92–36 ka	3	30,700 yr	Yang et al. (1999); Zhang and Li (2010)
Shuangshi-Xiling Fault	Northeast-trending strike-slip fault	57.4 ka–present	>1	<57,400 yr	Yang et al. (1999); Densmore et al. (2007)
Longriba Fault	Northeast-trending right-lateral strike-slip reverse fault	17.8–5.08 ka	4	4450 y	Ren et al. (2013)
Longquanshan Fault	Fold-and-thrust belt	90 ka–present	–	–	Deng et al. (1994); Wang and Lin (2017)
Maqin-Maqu Fault	Southwest left-lateral strike-slip reverse fault	–	–	–	Lin et al. (2002); Li (2009)
Awancang Fault	Northwest left-lateral strike-slip reverse fault	Late Quat.-0.85 ka	>4	<32,500 yr	Li et al. (2016)
Tazang Fault	Northwest left-lateral strike-slip fault	–	2 (2840 & 320 cal BP)	1420 yr	Fu et al. (2012)
Bailongjiang Fault	Northwest left-hand strike-slip reverse fault	17.4–0.6 ka	–	–	Huang et al. (2023)

Note: # Approximate recurrence is calculated by dividing the active period by the number of events.

3 Materials and Methods

In January 2019, we extracted a 166.4 m-long sediment core (DX-2) from the lowermost Tuanjie terrace, T1 (32°2′N, 103°40′E; Fig. 1c, 1d), using a percussive-rotary drill (1.5 m continuous core length, 88 mm diameter). The DX-2 core reached the base of the bedrock trough and was located 26 km down-valley from the upstream extent of the former palaeolake and 2 to 5 km from two tributary inputs. Core recovery was ~98% (~3 m of loss) (Fig. 2). The core was split lengthwise by a saw blade, and half was wrapped in plastic and stored at ~3°C. Cutting and photography were conducted at the Institute of Earth Environment, Chinese Academy of Sciences, Xi'an. We consider the SSDS identified in the central part of the core and exclude wall-induced disturbances associated with the coring process. Nine samples for optically stimulated luminescence (OSL) (Appendix 1) and thirty-one samples for radiocarbon (^{14}C) dating (Appendix 2) were collected to establish the chronological framework of DX-2, although the dating was unsuccessful.

4 Results

4.1 General core description

The DX-2 core was subdivided into three sections based on lithological characteristics (Fig. 2). The lower section (166.4–124.6 m) is characterised by cross-bedding and mainly comprises yellow to greyish-yellow coarse to fine sands, with larger rounded and scattered clasts (0.2–2 cm) near the base, as well as five units (4.17–0.17 m in thickness) consisting of angular clasts with 1-5 cm in size (Fig. 3a), interbedded with yellow clayey silt. These characteristics indicate that the lower section is mainly a fluvial environment with a short-term shallow lacustrine environment. The middle section (124.6–61.9 m) primarily contains dark grey to grey sandy silts, with some sporadic yellow sandy clays. This segment is mainly cross-bedded, plus three units (0.22–0.2 m in thickness) consisting of angular clasts with 0.5-2 cm in size (Fig. 3b). The upper section (61.9–0 m) consists of dark grey to grey clayey sands or clays and yellow sandy clays with abundant rhythmic varves. Except where beds are cross-bedded or deformed, the lamination is essentially horizontal. Based on the sedimentary characteristics, the middle and upper sections are interpreted as a lacustrine environment.

4.2 Soft-sediment deformation structures: description and interpretation

Based on visual characteristics and previous SSDS references, we identified at least 13 types of SSDS (Table 2), most frequently load and water escape structures, described as follows. Liquefaction represents the preservation of the original structure after grain mobility, while in the case of fluidisation, this original structure is not preserved (Kahle 2002). Hydroplastic deformation is characterised by water saturation and sediment cohesiveness and develops in incompletely lithified sediments when the fluid pressure is less than the weight of the particles (Kahle 2002; Alsop and Marco 2013; Valentine et al. 2020). Under the influence of differential compaction, pore pressure within the sediments varies. Sediments with a high compaction and low saturation tend to exhibit brittle deformation, such as fractured laminae, breccia clasts, normal and reverse faults (Kahle 2002; Druguet et al. 2009), whereas those with low compaction and high saturation display ductile deformation (Mohindra and Bagati 1996; Rossetti 1999; Rossetti and Góes 2000; Neuwerth et al. 2006), for example, folds (Kahle 2002; Druguet et al. 2009). Ductile and brittle deformation may coexist, with the transition from ductile to brittle behaviour primarily driven by vertical driving forces (Rodríguez-Pascua et al. 2000).

4.2.1 Load structures

The load structures in DX-2 include load casts, droplets, ball-pillow structures, and injection structures (dome and flame-shaped) (Anketell et al. 1970; Alfaro et al. 1997; Pandey et al. 2009).

Load Casts. These tend to occur along lithological boundaries in the upper and middle sections of the core. The large load casts (Fig. 4a) consist of several deformed laminae, which include complexes of smaller symmetrical or asymmetrical deformations with upturned curved morphology and have minor fractures inside or outside, with a total thickness of 10–25 mm and a width of 55–75 mm. Small load casts lack continuity (Fig. 4b) and are irregular and asymmetrical. The thickness varies between 2 and 15 mm. Some load casts fill with a mix and aggregation of surrounding sediments. For example, the load casts in Fig. 4c have a mixture of

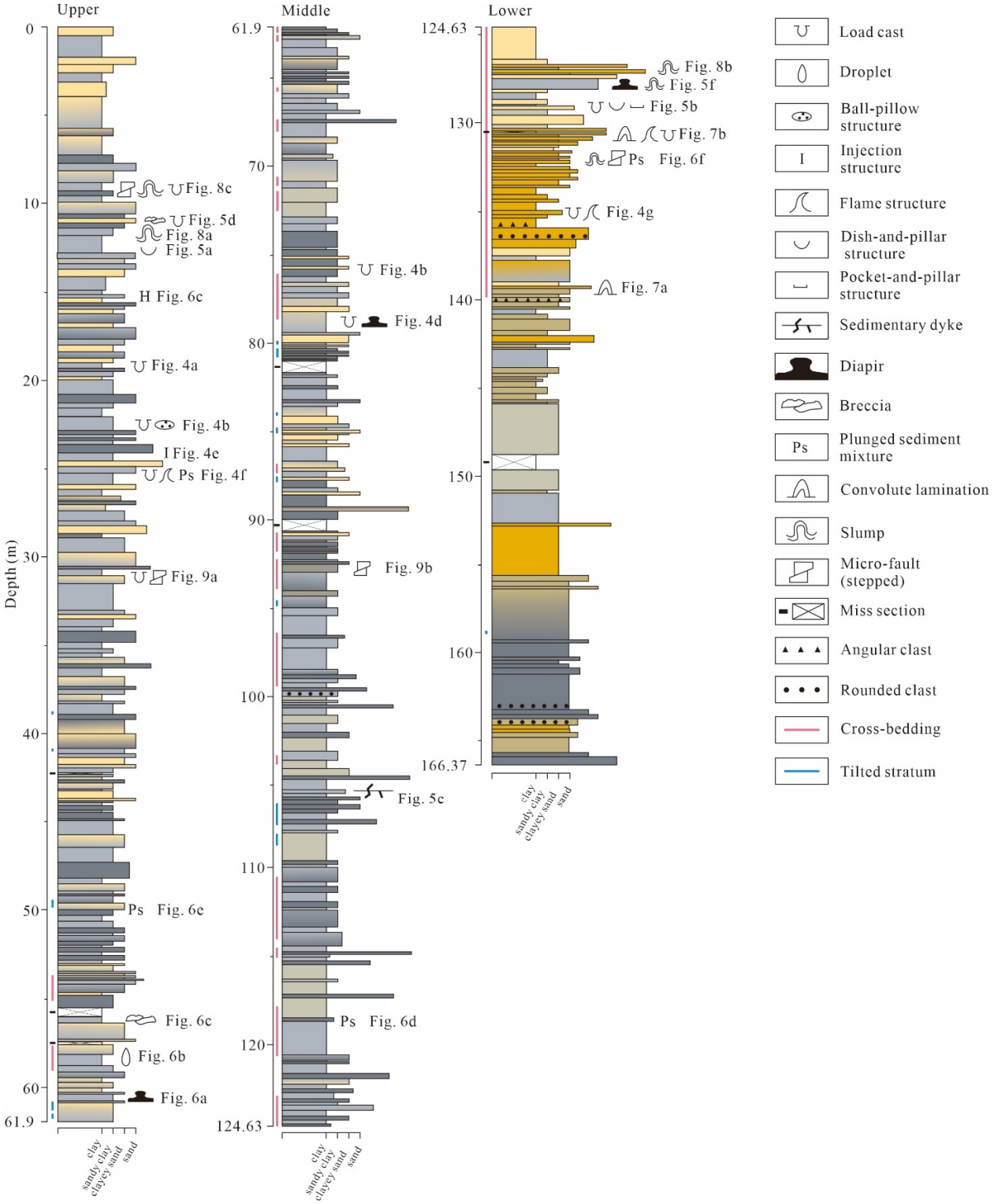

Fig. 2 Stratigraphic column of core DX-2 and the SSDS discussed in this paper (colours approximate those observed within the core).

yellow and dark grey coarser sediments. The thickness varies between 3 and 10 mm.

Load casts are denser sediments that sink into the underlying strata, triggered by liquefaction in a gravitationally unstable density gradient. Load casts always occur at the sand-mud interface with reversed density gradients (Sims 1973; Ghosh et al. 2012). These structures point to a rapid disturbance event that

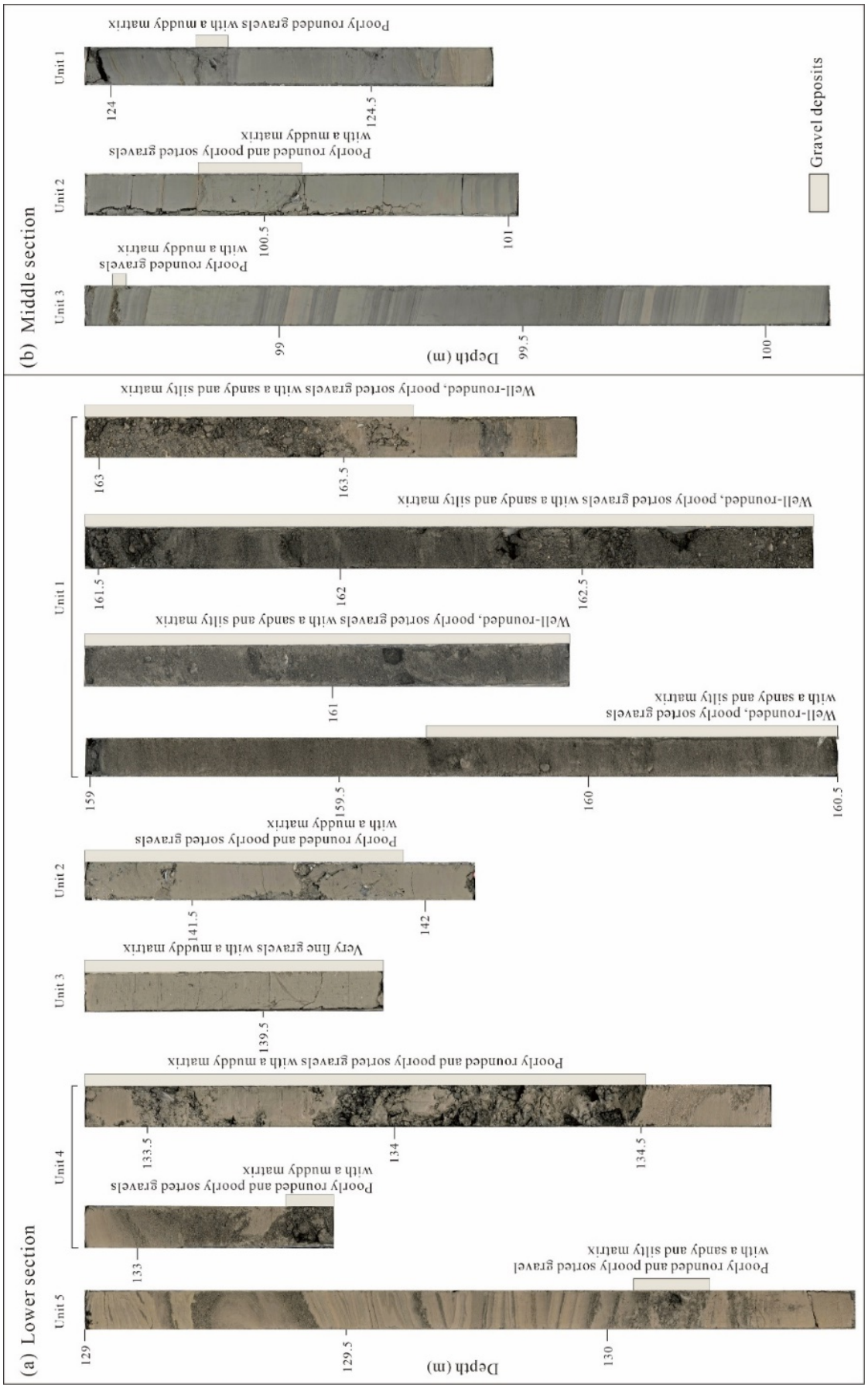

Fig. 3 Photographs of gravel units within DX-2, including generalised sedimentological descriptions: (a) gravel units in the lower section; (b) gravel units in the middle section.

Table 2 Proposed relationships between SSDS type and earthquake intensity based on previous studies

SSDS types		Modified Mercalli Intensity#	Presence in DX-2	References
Hydraulic structures		>X	No	Obermeier (1996); Zhang et al. (2007)
Breccias		>IX	Yes	Obermeier (1996); Rodríguez-Pascua et al. (2000); Zhang et al. (2007)
Load structures	Ball-pillow structures	>VIII	Yes	Rodríguez-Pascua et al. (2000)
	Droplets	>VI	Yes	Alfaro et al. (1997)
	Load casts	>VI	Yes	Alfaro et al. (1997)
	Injection structures	>VI	Yes	Topal and Özkul (2014); Deev et al. (2019)
Slumps		>VII	Yes	Calvo et al. (1998); Alsop and Marco (2013); Gladkov et al. (2016)
Sand volcanos		>VI~VII	No	Monecke et al. (2007); Brandes and Winsemann (2013)
Water escape structures	Dish-and-pillar structures	>VI	Yes	Neuwerth et al. (2006)
	Pocket-and-pillar structures	>VI	Yes	Neuwerth et al. (2006)
Plunged sediment mixtures		>VI	Yes	Rossetti et al. (2011)
(Micro-) faults		>VI	Yes	Marco and Agnon (1995); Rodríguez-Pascua et al. (2000)
Sedimentary dykes		≥VI	Yes	Rodríguez-Pascua et al. (2000); Kahle (2002)
Diapirs		≥VI	Yes	Rodríguez-Pascua et al. (2000)
Recumbent folds		>VIss	No	Sims (1973)
Convolute laminations		VI	Yes	Obermeier (1996)
Reclined folds		VI, IV	No	Obermeier (1996); Alsop and Marco (2013)
Undulate deformations		≤V	No	Rodríguez-Pascua et al. (2000)
Loop bedding structures		≤V	No	Rodríguez-Pascua et al. (2000); Kahle (2002)
Micro-folds		IV	Yes	Alsop and Marco (2013)

Note: # Earthquake magnitude (M) given in each reference has been converted to the Modified Mercalli Intensity (MMI = 0.92 + 1.29 M) (Gu 1983).

triggered liquefaction and fluidisation (Moretti et al. 2001), or differential loading, caused by the variation in the lateral thickness of the overlying bed (Ghosh et al. 2012).

Droplets. These occur in homogeneous clay or sand layers in the upper and middle sections of DX-2. All structures appear to be 'dripping' into the underlying sediments. These structures exhibit characteristics of downward extension, and the distorted height is much larger than the width. Several droplets appear to sink in different directions in two forms (Fig. 4d): (1) typical drop-shapes 2–10 mm in length and attached to the host layer (i.e., droplet-1); and (2) the droplet has a downward swing and tortuous shape detached from the host layer with lengths of 2–15 mm (i.e., droplet-2).

Droplets are formed as coherent sediment packages sink through a liquefied bed (Owen 1996; Ghosh et al. 2012). Depending on the specific orientation of droplet-2 forms, the vertical, slanting, and bending patterns indicate that the time-variable liquefaction pressures swing or displace laterally either randomly or systematically in one direction (Qiao and Guo 2011).

Ball-pillow Structures. These appear in the upper and middle sections of the core and coexist with load structures. Some structures are physically connected to the host sediments, while others have become detached. The horizontal and vertical axes are 3–10 mm and 3–7 mm, respectively. In Fig. 4b, the ball-pillow structure exhibits a concave-upward body, intruding internally with some lateral external margin erosion.

These structures were caused by the liquefaction of the underlying fine particles (Weaver and Jeffcoat 1978), and the reverse density loading might be an important deformation factor (Rossetti 1999). Due to long-term liquefaction, coarser overlayers were repeatedly detached to form ball-pillow structures in the fine strata (Owen 2003). Overlying sediments sink under shear vibration and gravitational action (Qiao and Li 2008).

Injection Structures (Dome, Flame). In DX-2, injection structures mainly appear as pillars, cones, and domes, with an injected height of 2–20 mm. The underlying lighter-coloured sediments are emplaced upward into dark, thin lamina, causing dome-like

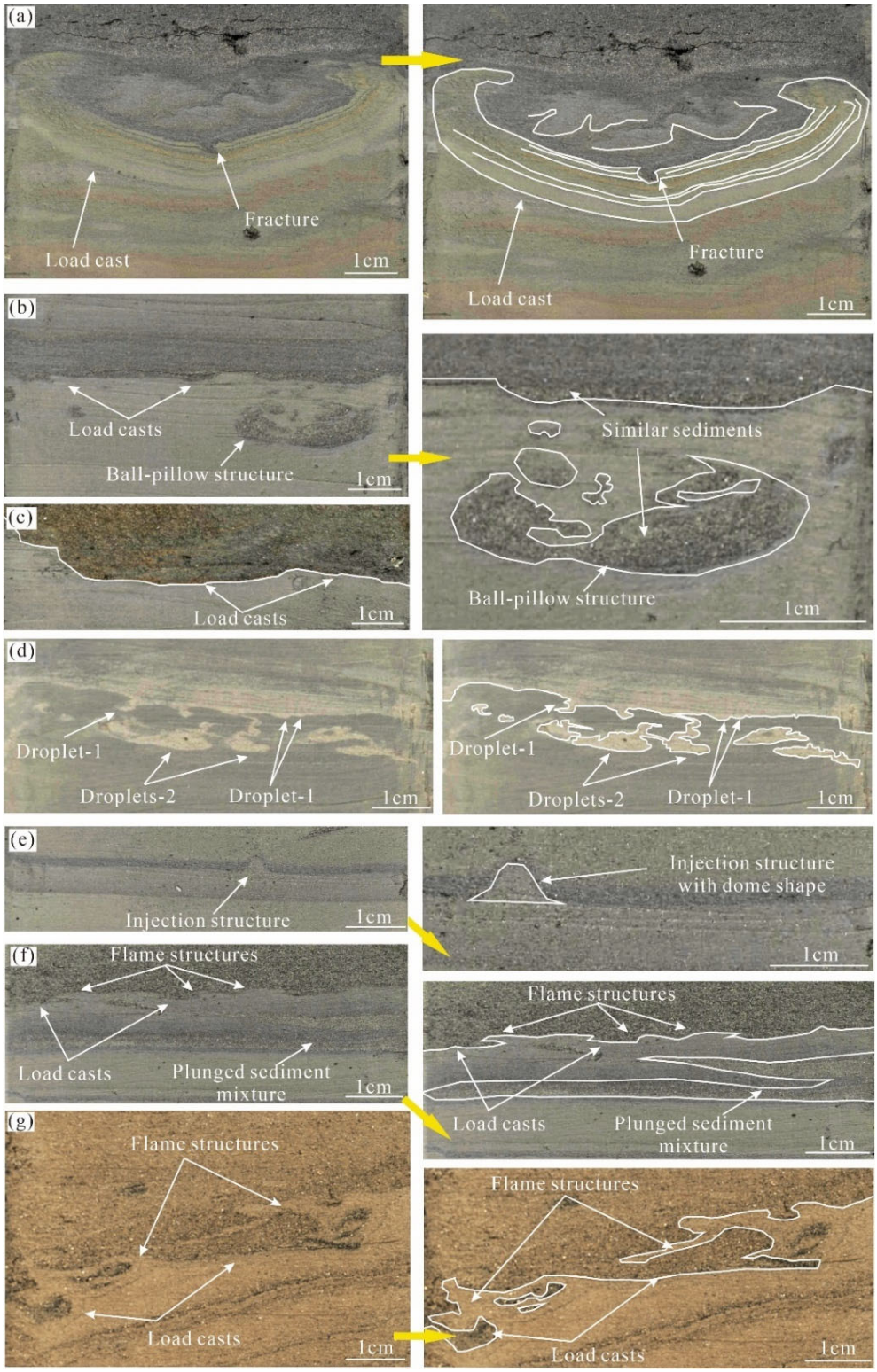

Fig. 4 Load structures: (a) larger load cast with a minor fracture inside; (b) small load cast and ball-pillow structure with a concave-upward body intruding internally with some erosion of the lateral external margins; (c) load cast with yellow and dark-grey coarser sediments mixed in the sinking area; (d) 'droplet-1' with typical drop-shape, and 'droplet-2' with a downward swing and tortuous shape; (e) injection structure with a dome shape, and dark laminae deformed by upward incision; (f) flame structures with irregular features associated with load casts (lighter, coarser sediments invade the finer sediments to form a plunged sediment mixture); (g) flame structures characterised as roll-up layers with sharp fractures.

protruding deformations (Fig. 4e). Flame structures are typical injection structures distributed widely throughout the core. The fine sediments invade the coarser layers, characterised as roll-up layers with sharp fractures (Fig. 4f). In the case of inclined bedding (~10°), flame structures are inclined towards the slope (Fig. 4g).

Injection structures form due to the rapid increase of pore-water pressure that exceeds the overlying sediments' lithostatic stress and tensile strength (Molenaar et al. 2021). As the pore-water content and pressure increase, flame structures may result from partial liquefaction and remobilisation (Lee and Phillips 2008) caused by unequal loading or high instantaneous sedimentation rates (Moretti et al. 2001; Gladkov et al. 2016; Deev et al. 2019). The deformation associated with inclined bedding (~10° in Fig. 4g) infers rapid deformation before consolidation (Lowe and Lopiccolo 1974; Rana et al. 2013), influenced by vibration or gravity, while the overlying sand layers slide along shear planes.

4.2.2 Water escape structures

Water escape structures, such as dish-and-pillar and pocket-and-pillar structures (Owen 2003), are scattered throughout the whole core.

Dish-and-Pillar Structures. These structures have a thickness of 2–5 mm and a width of 10–15 mm. The dish structures in Fig. 5a are lighter than the background sediments, which are strongly concave-upward, with discontinuous and irregular spaces. A narrow layer has been inserted beneath the left-hand dish structure, giving it a left-leaning shape; the middle one has a typical dish form, strongly concave-upward and approximately 5 mm in height; the dish structure on the right is a flat layer. The dish structure in Fig. 5b is a single coarser deformed layer that appears with pocket-and-pillar structures; both ends of this structure curve inward.

Water escape structures represent fluidisation and liquefaction that occurred shortly or long after the initial deposition (Obermeier 1996). These are common in fine- to medium-grained sand layers with high instantaneous sedimentation rates (Lowe 1975). The coarser particles have high permeability due to the large pore spaces but offer considerable mass resistance to lifting and fluidisation (Lowe 1975). The similar characteristics of the dish structures in Fig. 5a suggest they were initially flat laminations that were later disrupted during mass flow (Stauffer 1965, 1967). The disturbance may be caused by inhomogeneous shearing, internal load deformation, or localised water expulsion before or during consolidation (Stauffer 1965, 1967).

Pocket-and-Pillar Structures. These structures have heights and widths of 0.3–5 mm and 10–20 mm, respectively. In Fig. 5b, multiple thin laminae (3 cm) and four rows exhibit similar flat, broad, regular, and gently concave-upward characteristics, while the deformation weakens from bottom to top. The lower pockets have the same deformed features, while the upper pockets are right-leaning with irregular forms and are flatter than the lower ones. Eighteen cm-thick homogeneous dark sediment layers overlie the pocket structures featuring a defined and deformed boundary.

Pocket-and-pillar structures resemble dish structures with flat, broad, regular, and gently concave-upward characteristics (Neuwerth et al. 2006). The overlapping generations of pocket structures with flat morphology and a small dish (Fig. 5b) are related to rapid and high energy expenditure (Lowe and Lopiccolo 1974), high discharge rate (Lowe 1975), and uneven loading (Rana et al. 2016). The upper pockets are inclined due to asymmetrical rapid deposition, which may be contemporaneous with the formation of the lower pockets or due to a subsequently applied force.

4.2.3 Sedimentary dykes

In the middle section of DX-2, three ~10 mm long yellow sandy dykes invade both the upper and lower strata with upward- and downward-tapering shapes (Fig. 5c). Well-preserved source beds provide the sediment filling the dykes.

Fluidised sediments are quickly injected upwards or downwards due to increased water pore pressure (Brandes and Winsemann 2013; Zheng et al. 2015; Ezquerro et al. 2016; Törő and Pratt 2016; Chakraborty et al. 2019). Hydraulic fracturing and hydrodynamic pressure within the local strata make the pattern and orientation of dykes somewhat random (Obermeier 1996). The coarser yellow sand sediments readily penetrate the surrounding deposits under abnormal pressure (Zheng et al. 2015), fill the fractures, and are ultimately preserved by dehydration and compaction (Picard and High 1972; Tanner 1998; Montenat et al. 2007; Harazim et al. 2013). Otherwise, the sudden loading of sediments can also cause downward dykes to form (Törő and Pratt 2015).

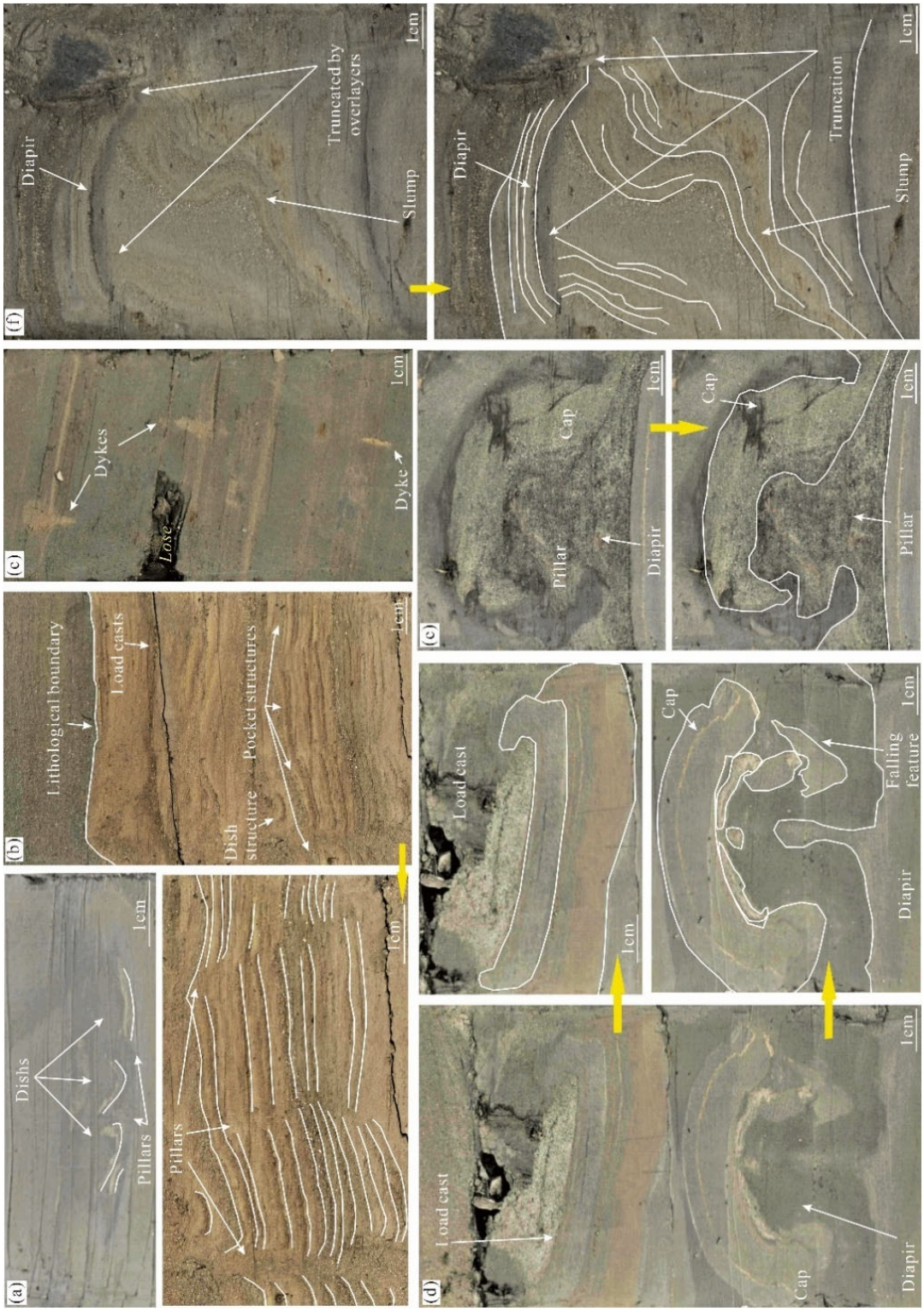

Fig. 5 Water escape structures, sedimentary dykes and diapirs: (a) dish-and-pillar structures, three dishes with strongly concave-upward, discontinuous, and irregular spaces; (b) pocket-and-pillar structures showing four rows with deformation weakened from bottom to top, the lithological boundary separates light brown and dark grey sediments; (c) three sedimentary dykes connecting to their source layer, with upward and downward shapes (some material was lost during core splitting); (d) diapir shows as a 'cap' suspended in the background sediments (with falling inner layer of this cap), the load cast can be seen in the overlying strata; (e) diapir with a mushroom-shaped 'cap' and 'pillar', the sandy pillar intrudes the overlying cap; (f) slump develops on a slope, has significant irregular, crimp features, and is truncated by the overlain multiple laminae, which formed as a diapir.

4.2.4 Diapirs

Diapirs mainly occur within silt-rich clay or sandy layers in the upper section of the core. They appear arch-shaped, mushroom-shaped (Fig. 5d, 5e), and cone-shaped (Fig.5f), with the entire diapir height ranging from 16 to 50 mm and a width between 20 and 50 mm. The mushroom-like diapirs consist of two parts: the 'pillar' and the 'cap' (Fig. 5d,5e). The background fine-grained sediments moved from both sides toward the middle, making the clayey cap appear isolated and suspended. However, the inner laminae of the cap detached from the host sediments and moved downward, which resembles a collapsing phenomenon, while the underlayer is extruded into the background sediments toward the cap (Fig. 5d). The sandy pillar clearly intrudes into the overlying sediments, which formed as a cap that is influenced by the pressure from the upper and lower sediments. The cone-shaped diapir has upward-curved laminae coexisting with the slump structure (Fig. 5f).

Fluidisation can cause the source sediments to move upward, forming a cap and a pillar shape (Berra and Felletti 2011; Ezquerro et al. 2016). The collapse beneath the cap (Fig. 5d) may be triggered by dewatering-generated sediment movement towards the upper laminae (Rodríguez-Pascua et al. 2010). The presence of sand intrusions above is evidence of shear (Fig. 5e), indicating that the structure is caused by injection under pressure and squeezing upward (McLaughlin and Brett 2004). Arched-shaped and cone-shaped diapirs may be caused by shaking and increased pore pressure of background sediments (Zheng et al. 2015; Chakraborty et al. 2019).

4.2.5 Breccias

Breccias are distributed sporadically throughout the DX-2 core; we observed three types. In the upper section, Type 1 breccias develop as independent structures, while in the middle and lower sections of the core, they coexist with other structures. Type 1 breccias have been fractured with minor dislocations, yet the original morphology is still evident (Fig. 6a). The thickness ranges from 25 to 350 mm. Type 2 breccia has a diameter of about 35 mm and is observed *in situ*; two breccias overlap and are tilted slightly to the left (Fig. 6b). Type 3 breccia is developed in an 80-mm-thick layer of dark sediments, with a diameter of 7–43 mm (Fig. 6c).

Type 1 breccias have a thicker original structure, inferring a sudden increase in pore-water pressure to the static confining pressure triggered by continuous cyclic shearing, which led to liquefaction (Obermeier 1996; Zhang et al. 2007). The overlapping two breccias (Type 2) were caused by the pressure of pore water being released upward and the fluidisation of the top sediments (Agnon et al. 2006), which may be triggered by shaking or water escape from the underlying uncompacted sediments (Fig. 6b). The disordered dispersion of breccias (Type 3) may be triggered by strong shaking (Fig. 6c) (Agnon et al. 2006).

4.2.6 Plunged sediment mixtures

Plunged sediment mixtures are present throughout the core. These sediments intrude into two different sedimentary units, both vertically and horizontally, finally appearing as columnar and wedge-shaped intrusions. In Fig. 6d, the dark sandy sediments are the host sediments, and some of them have fragmented during descent and formed as clumps that float within the dark clay layer. Some dark sandy sediments not only intrude vertically into the underlying clayey layer but also spread laterally and interlayer with the lighter underlying layer, finally appearing as wedge-shaped intrusions (Fig. 6e). Some of the underlying clay beds in this SSDS float within the friable overlying sands (Fig. 6f). The vertical depth ranges from 7 to 83 mm.

The underlying sediments are invaded and filled by the overlying sandy layer, indicating a time lag between sediment deformation and consolidation (Rossetti et al. 2011). Sediment intrusion and mixing are related to liquefaction and sediment collapse triggered by external forces, such as lower-energy vibrations (He et al. 2011).

4.2.7 Convolute laminations

Convolute laminations are distributed throughout the core. The deformation thickness fluctuates from 40 to 170 mm. Convolute lamination lacks uniform axial planes and mainly exhibits inclination angles of about 20°–30° (Fig. 7a). Multiple layers with different particle sizes and irregular features are faintly visible at the base, while the upper section mixes with the background sediments. A special convolute lamination developed in the lower part of DX-2, with a diameter of 250 mm, is associated with load casts and flame structures (Fig. 7b). The inner core is made up of tortuous clayey layers that gradually coarsen outward, while a clay layer wraps around the outer perimeter.

Convolute laminations occur when pore pressure exceeds hydrostatic pressure under rapid deposition

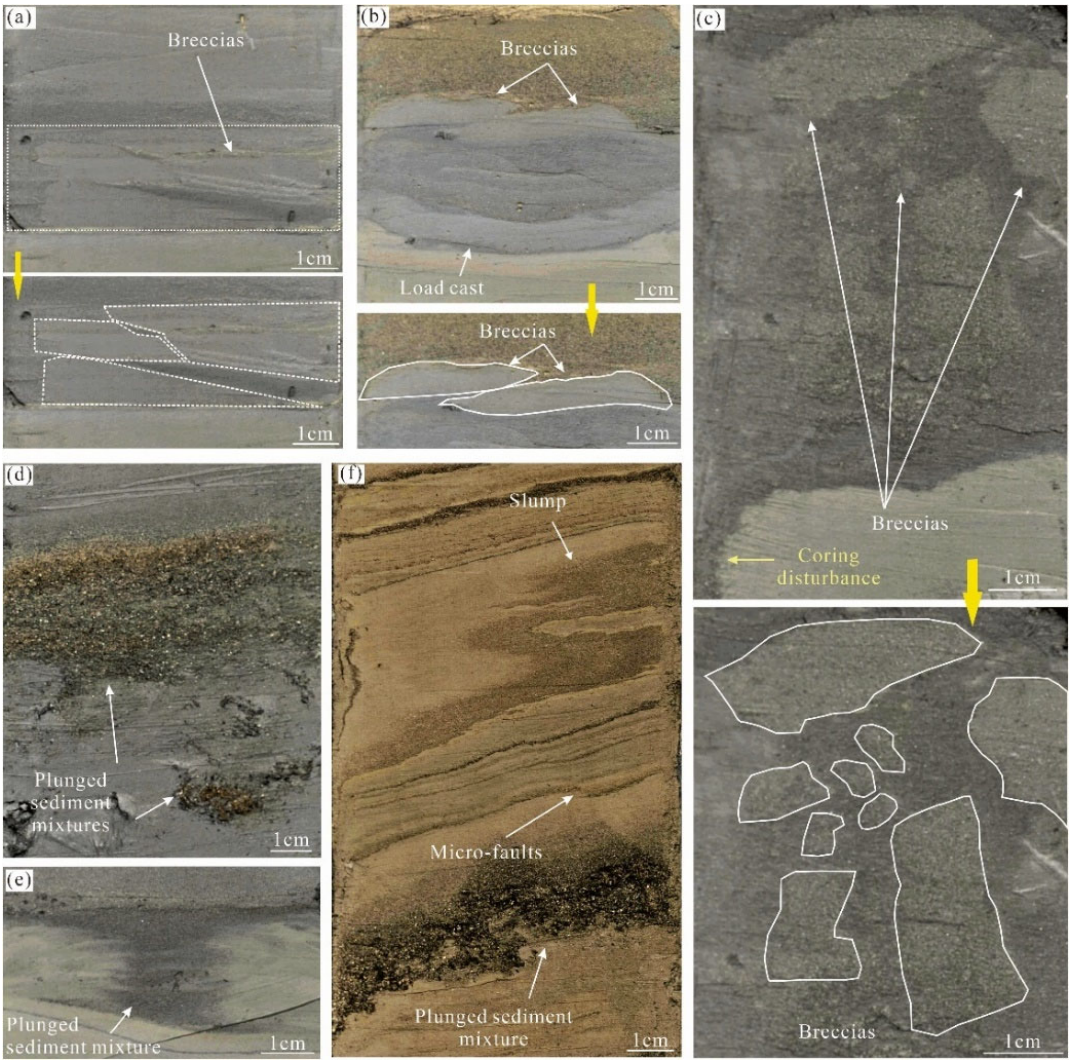

Fig. 6 Breccias and plunged sediment mixtures: (a) type 1 breccias *in situ* with slight dislocation; (b) type 2 breccias overlapping with a load cast; (c) type 3 breccias suspended in dark sediments with sub-angular to angular morphology (note some disturbance during coring); (d) vertically-plunged sediment mixtures showing coarser sandy particles intruding the neighbouring sediments and mixing with underlying clayey layers; (e) wedge-shaped plunged sediment mixture, with dark coarser sediments intruding downward and mixing with the lateral clayey sediments; (f) basal coarse particles shown invading downwards to form a plunged sediment mixture, overlain by two graded bedding micro-faults and an irregular/inhomogeneous slump.

conditions, resulting in partial liquefaction during or following deposition (Allen 1977; Middleton et al. 2003; Gladstone et al. 2018). The inclined deformations are subject to the combined effects of vibration and gravity, with stratal inclination controlled by the evolution of the lake basin sedimentary infill or subaqueous slope failure (Zhong et al. 2017). The convolute lamination is inclined ~20° to the left, indicating that the external force acts from left to right (Fig. 7b). The large, round, and inner tortuous laminae indicate post-depositional hydroplastic deformation with a lower limit of foundering and deformation (Wallace and Eyles 2015). It may be formed by the flow and shear of fine-grained layers within the convolute laminations (Gladkov et al. 2016) or by load pressure and sliding along the slope (Zheng et al. 2015).

4.2.8 Slumps

Slumps with thicknesses ranging from 10 to 120 mm occur within the upper and lower sections of the core. In Fig. 6f, the slump structure consists of clayey and silty-clay layers with irregular and inhomogeneous characteristics. Three clayey, thin layers bend upward, with a weak-moderate intensity and asymmetry, exhibiting thinner long limbs and thicker short limbs (Fig. 8a). The deformed layers of micro-folds are

characterised by irregular, uncoordinated, and poorly oriented layers (Fig. 8b). The slump in Fig. 8c develops in load casts, where light clayey sediments form superimposed hummocks. The underlying loaded laminae have a fissure on the right side. In Fig. 5f, the slump develops on slopes (about 30°–45°) with significant irregular and crimp deformations and is truncated by overlying multiple laminae.

Slump structures reflect load and overpressure caused by sudden and rapid external forces (Sieh 1978; Holzer et al. 1989; Obermeier et al. 1990). Slumping can also stem from different density gradients near the sediment-water interface (Pandey et al. 2009). These structures are caused by increased pore-fluid pressure from particle movement (Gladkov et al. 2016). The fissure on the right side of the load cast (Fig. 8c) indicates rapid hydraulic drawdown when sediments fall out of suspension (Obermeier et al. 1990; Alsop and Marco 2013). Especially frequent where the slope angle steepens to 30°–45°, with multiple laminae truncating slump features, this SSDS may be caused by hydroplastic deformation or rapid water flow at the sediment-water interface (Fig. 5f) (Koç Taşgın 2011; Alsop and Marco 2013).

4.2.9 (Stepped) Micro-faults

Micro-faults are distributed throughout the core. These may dislocate a single lamina or disrupt SSDS (Fig. 9a) with a 3–60 mm displacement distance. In Fig. 6f, two micro-faults occur on the right side of two coarser layers. Each layer is characterised by graded bedding, and the left part of these two layers exhibits the same

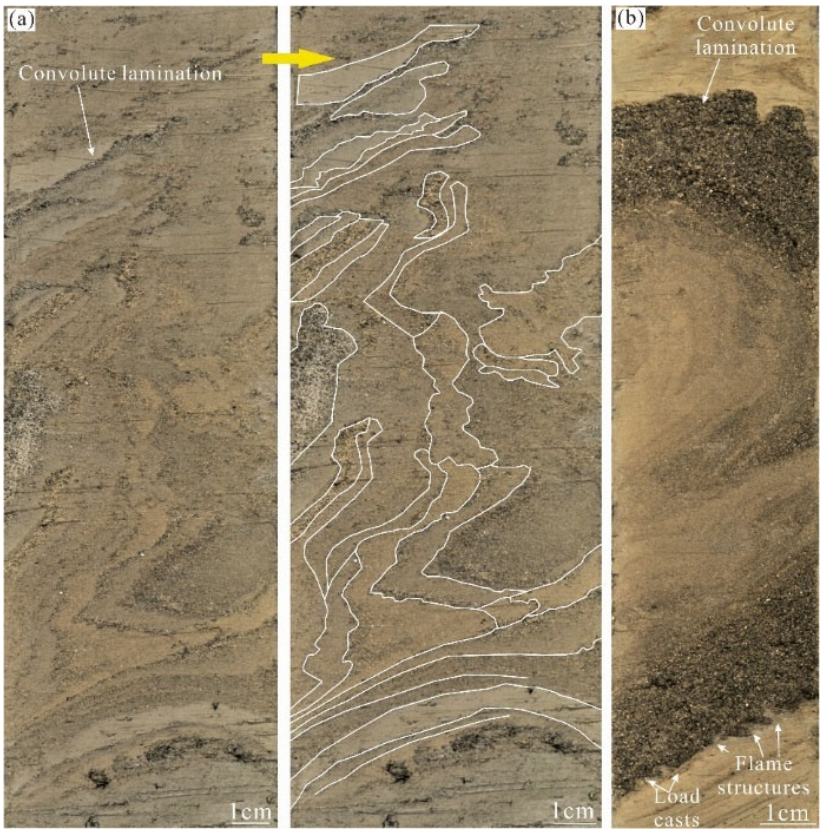

Fig. 7 Convolute lamination: (a) convolution laminations lacking uniform axial planes and with different particle sizes and irregular features, while the upper section mixes with background sediments; (b) inner core of convolute lamination made up of tortuous clayey layers that gradually coarsen outward, while a clay layer wraps the outer perimeter.

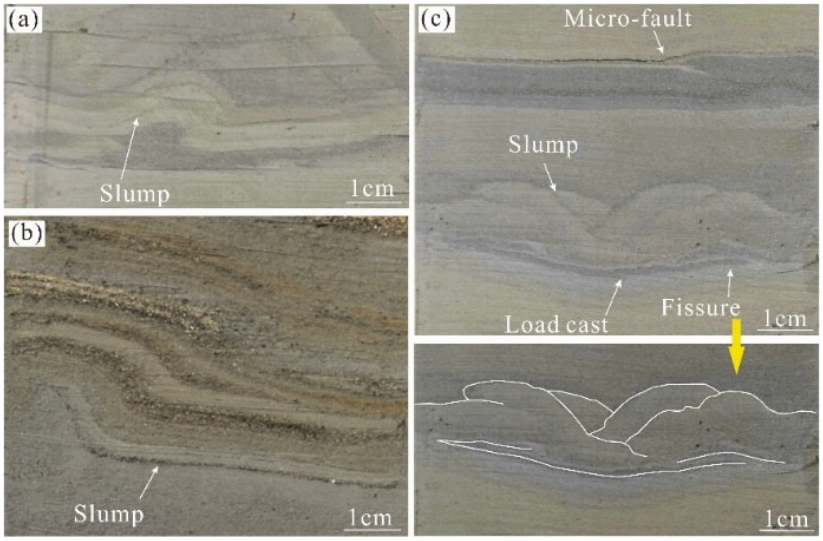

Fig. 8 Slumps: (a) Slump has thinner long limbs and thicker short limbs. The dark, coarser sediments mix with lighter background sediments on the left side and fill beneath the slump; (b) slump within layers of different granularity, the layers characteristically are irregular, uncoordinated, and poorly oriented; (c) The underlying loading lamina has overlapping features on both sides, with a fissure on the right side. In addition, there is a micro-fault in the overlying layer.

deformation. In Fig. 9a, the original light layer contains one dark lamina surrounded by dark, coarser sediments. This layer breaks into four fragments with clearly defined displacements. These pieces overlap from left to right. The middle two have prominent 'S'-shaped deformation features.

Stepped micro-faults occur in the middle section of the core. The vertical dislocation distance is 1–4 mm, and the entire thickness ranges from 30 to 50 mm. The faults cut through multiple layers with 5°–10° inclinations arranged in disorder (Fig. 9b).

In general, micro-faults occur due to the compression of the sediment body by water at depth (Seilacher 1969) and reflect specific properties of the sediment, such as graded bedding (Fig. 6f) or laminations (Fig. 9b). A disharmonic micro-fault indicates a higher pore-water content and pressure during folding, pore water is reduced after folding, and then brittle displacement. The overlapped feature results from the liquefaction and remobilisation of coarser particles (Fig. 9b) (Lee and Phillips 2008). There are two types of micro-faults that external forces may induce: (1) brittle deformations caused by sudden pressure or uneven stress, where the layer cuts off without any other deformation and deforms *in situ*, and (2) ductile and brittle deformations with the morphologies of truncated and dislocated movement, reflecting brittleness and shear. This transition from ductile to brittle deformation records the decline in water content due to progressive compaction (Rodríguez-Pascua et al. 2000; Lee and Phillips 2008).

4.3 Geochronology results

Our efforts to apply optically stimulated luminescence (OSL) and radiocarbon (^{14}C) dating to the DX-2 were largely unsuccessful (see Supplementary Information). The measured depositional ages range from ~173 to 17 ka, and there is no convincing relationship between age and stratigraphic depth in the core (Appendix 3). In the case of the OSL and possible sediment reworking, it appears the sediments were inadequately bleached by sunlight before deposition. Our samples for radiocarbon dating were limited to the organic fraction extracted from bulk sediment in the core. The radiocarbon in such samples typically derives from allochthonous and autochthonous sources that integrate different timescales, leading to erroneous depositional ages (Strunk et al. 2020).

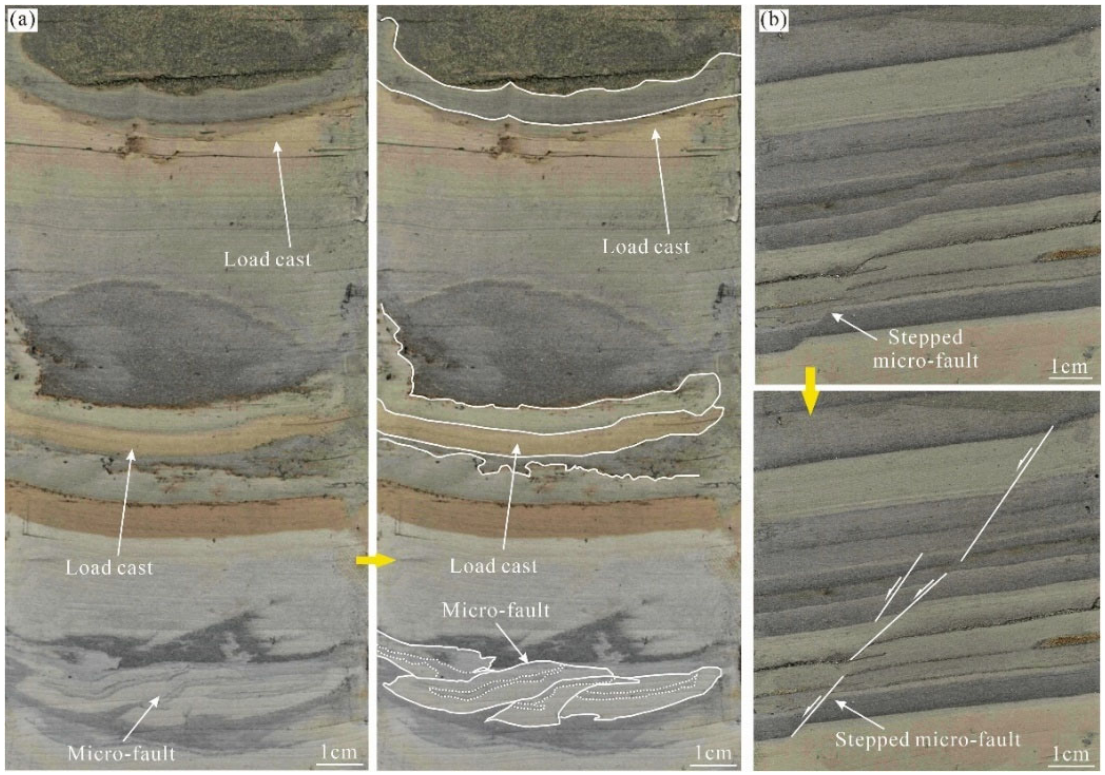

Fig. 9 Micro-faults: (a) micro-fault showing four fragments with clearly defined displacements; fragments overlap from left to right (the middle two have prominent 'S'-sharped deformation) plus a load cast in the overlying strata; (b) stepped micro-fault cutting across inclined planar bedding.

We can estimate the age span of the Diexi lacustrine sequence if we accept the bottom-most radiocarbon date (35.13 cal ka BP) from the ZK-2 drill core (Fig. 1d) published by previous workers (Wang et al. 2012; Wang et al. 2020). The ZK-2 core is located at a slightly higher position in the sedimentary sequence, but by extrapolating the mean sedimentation rate of 15 mm/yr (Wang et al. 2012) to the deeper position of the DX-2 core, we can obtain an estimate of ~41 cal ka BP for the initiation of the lacustrine sequence. Both cores share a common upper limit dated to ~27 ka (Li et al. 2024) when the Minjiang River cut a new course.

5 Discussion

5.1 Representativeness of the DX-2 SSDS record

As noted above, the geochronology did not yield reliable results for the DX-2 core, so we cannot precisely correlate it with the other major core extracted from Diexi Palaeolake, ZK-2 (Wang et al. 2012). Nevertheless, SSDS are also observed in other drill cores and sedimentary exposures from within and surrounding the Diexi Palaeolake. Four cores drilled at Tuanjie (Fig. 1d) and Jiaochang reveal at least ten disturbed layers formed in the interval 33–18 cal. ka BP (Wang et al. 2012) and several SSDS types are observed within sedimentary sections up to 26 km upstream of Diexi (Xu et al. 2020). For instance, at Shawan Village (5 km upstream of Diexi), seven deformed layers are OSL-dated to between 27–19 ka (Wang et al. 2011); and at Luobozhai Village (11 km upstream of Diexi), 18 SSDS-rich layers are dated (with OSL and ^{14}C) to 18–10 ka (Zhong et al. 2023). Moreover, lacustrine sections exposed near Tuanjie, Shawan, Taiping and Luobozhai (Fig. 1) also display notable perturbations. The depositional ages of SSDS in these outcrops are somewhat younger than those in the DX-2 core. Still, their presence further supports the idea that SSDS are widely distributed in unconsolidated deposits throughout the Diexi area and that the DX-2 core is the most comprehensive record of SSDS within the palaeolake from 41 to 29 cal ka BP.

In the following text, we review the occurrence of the various SSDS within the DX-2 core with respect to the likely driving forces and deformation mechanisms. We focus on identifying the most probable trigger mechanism that might explain repeated SSDS up the core throughout the lake's duration. While some success has been achieved in simulating seismically-induced SSDS via physical models (Kuenen 1958; Owen 1996; Moretti et al. 1999; Yan et al. 2007; Wei et al. 2015), it is fair to say that many SSDS remain enigmatic in terms of their genesis. Nevertheless, it is still possible to outline the physical principles that are likely to be at play to some extent, given that SSDS formation involves three fundamental conditions: (1) a driving force, (2) a deformation mechanism, and (3) a trigger mechanism (Owen and Moretti 2011). The driving force is the condition that deforms the original sedimentary features; the deformation mechanism is the specific agent by which the sediment is deformed; and the trigger mechanism refers to an event, condition or process that causes the deformation.

5.2 Driving forces

Considering the sedimentary environment of the SSDS observed in DX-2, we suggest that the driving forces of sediment deformation (Neuwerth et al. 2006; Owen et al. 2011; Moretti and Van Loon 2014; Molenaar et al. 2021) are mainly: (1) uneven loading at the irregular sediment-water interface (Fig. 4b); (2) gravitational inhomogeneity due to a reversed density gradient (Fig. 4f); (3) sliding or slumping caused by gravity on slopes (Fig. 8c); (4) shear stress caused by aqueous or other currents, such as cyclic shear (Fig. 6c), horizontal shear (Fig. 4g), vertical shear (Fig. 9b), compressive stress (Fig. 6f), or extrusion stress (Fig. 4d).

5.3 Deformation mechanisms

In the DX-2 core, SSDS occur in clayey and sandy sediments, which are susceptible to vibration (Calvo et al. 1998; Jones and Omoto 2000; Montenat et al. 2007; Pandey et al. 2009; Owen and Moretti 2011; Zheng et al. 2015). Water-saturated sediments with a highly impermeable clayey cap are easily deformed (Montenat et al. 2007). These loose sediments are prone to liquefaction, fluidisation, hydroplasticity, and brittle deformation under a given applied force (Jones and Omoto 2000; Koç Taşgın 2011; Owen et al. 2011; Zheng et al. 2015). The increase in pore-water pressure leads to liquefaction or fluidisation, and the free flow of sediments occurs during a complete loss of shear strength (Youd 1975; Field et al. 1982). The liquefaction and fluidisation deformations described from the DX-2 core are interpreted as being subject to

subsequent deformation mechanisms: vibration, dewatering, continuous cyclic shear, etc..

Conversely, hydroplastic deformations might occur in sediments that have not reached a sufficient degree of liquefaction. Brittle deformation occurs when pore water pressure exceeds the capacity of the sediments to consolidate. This deformation mechanism can be affected by sudden pressure or uneven stress. Furthermore, with the progression of lithification, purely ductile deformation transitions to a purely brittle deformation (Rodríguez-Pascua et al. 2000).

5.4 Trigger mechanisms

It is accepted that a wide range of mechanisms can potentially trigger SSDS. These include mass movements (Purvis et al. 2002; Shanmugam 2016), groundwater dynamics (Owen 1995; Massari et al. 2001; Rana et al. 2016), glacier activity (Hart and Boulton 1991; Lee and Phillips 2008; Jiang et al. 2016; Müller et al. 2021), tides (Greb and Archer 2007; Ettensohn et al. 2011; Törő and Pratt 2016), storms (Alfaro et al. 2002; Komatsubara et al. 2008; Chen and Lee 2013; Üner 2018), tsunamis (Le Roux et al. 2008; Bertran et al. 2019), overloading (Jones and Omoto 2000; Moretti and Sabato 2007; Üner et al. 2019), and earthquakes (Sims 1973; Allen 1986; Obermeier 1996; Rodríguez-Pascua et al. 2000; Ettensohn et al. 2011; Rana et al. 2013; Onorato et al. 2016; Azennoud et al. 2022; Bhadran et al. 2023). Identifying the origin of SSDS is challenging, as different triggering mechanisms can produce similar SSDS. We begin by surveying the range of potential triggering mechanisms likely to apply at Diexi.

5.4.1 Mass movement

Common mass movement types include slope failures, collapses, debris flows, plastic flows, and turbidity currents (Mulder and Cochonat 1996; Owen et al. 2011; Kremer et al. 2015; Shanmugam 2016). Massive sand beds are commonly observed in the mass movement-related SSDS, where the sands are poorly sorted with a 5–15% matrix. Floating mudstone clasts (angular, cm-diameter), primary basal glide planes, steep internal shear planes, and water escape structures represent the sedimentary characteristics of mass movement-generated deposits (Shanmugam 2016). SSDS, such as breccias, have been interpreted as products of mass movement (Törő and Pratt 2016). However, the spatially restricted core observations and the lack of lateral correlation archives make it difficult to distinguish large-scale in situ disruption from localised perturbations. Some SSDS are found in the coarse sand layers which may be related to mass movement (García-Tortosa et al. 2011; Törő and Pratt 2015). However, the layers of SSDS within DX-2 are always thin, so we believe this excludes deep-seated mass movements on the lake floor which tend to be associated with detachment surfaces which are absent in the DX-2 core.

5.4.2 Groundwater dynamics

Groundwater can be responsible for liquefaction deformation (Owen 1987, 1996; Moretti et al. 2001). The main types of groundwater-induced SSDS are cups, water escapes, and droplets, usually several metres thick (Owen 1995). In contrast, the thickest SSDS observed in DX-2 is only 480 mm; hence, the SSDS in our core do not appear to be the product of groundwater-induced vertical shear stresses (see Section 5.2). In addition, extensive liquefaction was not observed to form discrete and chaotic SSDS units, characteristic of upwelling groundwater (Owen 1995). Based on the above points, we rule out any significant influence of groundwater activity in the DX-2 core.

5.4.3 Glacier activity

The advance of a glacier leaves proglacial contractional structures and SSDS associated with extension and shear (Hart and Boulton 1991; Müller et al. 2021), and seasonal meltwater can cause repeated cycles of fracture-expansion-deposition, forming SSDS-like clastic dykes (Le Heron and Etienne 2005). Although there were three palaeoclimate transitions between ~40-30 ka (Zhang et al. 2009), no glacial sedimentary characteristics have been observed around the Diexi Palaeolake (Li et al. 1964); hence, we exclude the role of glaciers here.

5.4.4 Tides, storms and tsunamis

Tides, storms, and tsunamis occur along the margins of large water bodies (Greb and Archer 2007; Komatsubara et al. 2008; Üner 2018). They can form deposits from cm to m in thickness and span areas of 10^3 km^2 (Shanmugam 2016). Different triggering mechanisms will form specific sedimentary features in the strata near SSDS. Tide deposits are formed via reversing (bimodal) water current or cyclic oscillations (Miall 2000; Üner et al. 2019). Storm deposits are typically associated with erosion surfaces, graded

bedding, parallel lamination, wavy cross-bedding, hummocky cross-bedding, troughs and climbing ripples, shells, biogenetic escape structures, and gutter structures (Myrow and Southard 1996; Komatsubara et al. 2008; Panja et al. 2018; Üner 2018). Tsunami deposits generally consist of a return-flow unit, mud-cap and rip-up clasts, and massive or parallel-laminated structures (Nanayama et al. 2000; Morton et al. 2007; Komatsubara et al. 2008).

The Diexi Palaeolake lies in a mountain gorge. Its total area and length are 21.4 km² and 26 km, respectively (Dai et al. 2023). Tidal action and storm waves are unlikely to occur (Ezquerro et al. 2016; Törő and Pratt 2016) in such a long, narrow lake. However, tsunamis could plausibly be triggered by rock avalanches or rockslides that fall directly into the lake from the surrounding steep hillslopes. For example, the impulse wave induced by a rockslide-generated tsunami is known to form and propagate over up to 12 km (Miller 1960; Franco et al. 2020).

Although we cannot rule out the effects of rockslides instigating SSDS over vast areas, there are only eight units consisting of coarse-grained, unsorted angular clasts or poorly rounded, unsorted clasts within muddy matrix units. Five of these units occur in the lower section, three within the middle section and none in the upper section of the core. All these units are thin and thus unlikely to relate to large-scale basin-wide tsunamis, but rather could relate more readily to localised rockfall from bordering rock outcrops early in the development of the lake.

5.4.5 Rapid sedimentation

Rapid sedimentation is a common triggering factor for liquefaction in sand-on-sand and sand-in-clay systems (Moretti et al. 2001). It can cause liquefaction at great depths below the sediment-water interface. Diexi Palaeolake has experienced exceptionally fast sedimentation (~15 mm/yr) thanks to the extremely high sediment supply from seismically perturbed hillslopes and rivers feeding into the lake (Wang et al. 2012). In the DX-2 core, some small-scale sand-clay SSDS can be considered a product of rapid sedimentation (Moretti and Sabato 2007; Azennoud et al. 2022). However, we note that all the SSDS are of limited thickness (0.5–800 mm) and are most likely generated prior to becoming deeply buried in the sediment pile.

5.4.6 Earthquakes

SSDS are widely observed in seismically active regions. In the upper Minjiang River, including the Diexi area, SSDS are considered the product of earthquakes (Wang et al. 2012; Jiang et al. 2014; Xu et al. 2015; Jiang et al. 2016; Zhong et al. 2019; Shi et al. 2022; Zhong et al. 2022). Furthermore, the irregular recurrence of various SSDS types in the vertical sequence of the DX-2 core (Fig. 10) are a signature of seismicity (Hilbert-Wolf et al. 2009; Üner 2014; Ko et al. 2017). The high frequency of seismicity in the Diexi area has also been identified via high-resolution geochemical profiling; for example:

Eight earthquakes are recorded between 20.2 and 12.6 ka, with only two events before 16 ka and six after 16 ka, suggesting an increased frequency over time (Mao 2011).

During the interval 20–8 ka, 26 earthquakes may have been recorded at Tuanjie and 23 at Taiping, while 10 possible events were recorded at Shawan between 15 and 10 ka (Zhong 2017).

Between 18.6 and 10 ka, 30 earthquakes were recorded at Tuanjie (Zhong et al. 2024).

The Luobozhai section, which spans 18–10.2 ka, recorded 35 earthquakes (Zhong et al. 2023).

Based on previous assessments, the minimum earthquake magnitude required to trigger SSDS is M 5 (Table 1) (Atkinson et al. 1984; Audemard and Santis 1991; Marco and Agnon 1995; Deev et al. 2019;

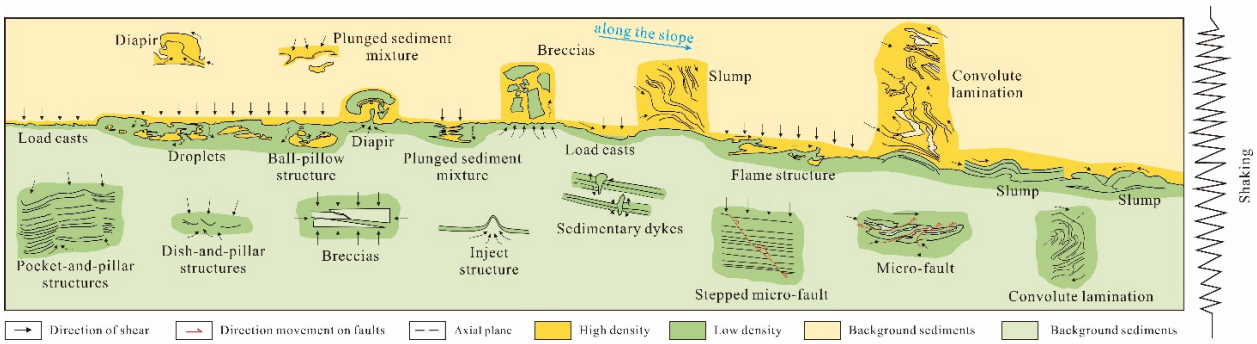

Fig. 10 Cartoon showing various SSDS of DX-2 formed during seismic shaking.

Molenaar et al. 2024 and papers in Table 2). A magnitude threshold of 5 (~VII–VIII in Modified Mercalli Intensity, MMI, Gu 1983) has been comfortably exceeded multiple times in the upper Minjiang River since 1930. The 1933 event was M 7.5, and 57 earthquakes have been recorded with M ≥ 4.7, including 18 of M ≥ 6.0 (Chai and Liu 2002; Ma 2017). Given this high frequency of seismic shaking and the occurrence of numerous nearby faults (Fig. 1b) active over the period during which the Diexi lacustrine sequence accumulated, it would be rather odd if earthquake signatures were not recorded within the DX-2 core.

We note that for earthquakes of M ≥ 7.0, soft sediments can potentially liquefy even 100–200 km from the epicentre (Field et al. 1982; Ambraseys 1988; Obermeier 1996; Gibert et al. 2011; Ghosh et al. 2012; Wallace and Eyles 2015; Deev et al. 2019). Farther afield from Diexi (in Lixian County, 83 km away), 70 earthquakes have been reported between 19 and 6 ka, including at least four M > 7 (Jiang et al. 2016; 2017), in addition to the M 7.0 earthquake in Jiuzhaigou, which is 150 km from Diexi (Fan et al. 2018). Large, frequent earthquakes such as these over the past century are undoubtedly sufficient to deform unconsolidated sediments (Rodríguez-Pascua et al. 2000).

5.5 Model of earthquake-induced SSDS formation through time

The results and discussion above show that distinct thin layers of disrupted sediments occur at irregular intervals throughout the DX-2 core. However, it is important to note that these units account for only 9% of the core length, whereas the remaining 91% represent essentially undisturbed lacustrine deposition. Cross-bedding, as is commonly related to an active fluvial current leading to aggradation, is more common in the lower section of the core, reduces in the mid-core and is absent in the upper section, which contains mainly regular laminations consistent with quiescent lacustrine conditions. This gross trend in sedimentation is consistent with the accumulation of sediments within a deepening lake, such that the fluvial influence on deposition declined with time. Concomitantly, rockfall from the confining rocky slopes apparently also became less frequent, as indicated by the fewer angular clasts horizons up the core.

Within this general pattern of sedimentation through time, the presence of discrete layers of SSDS may be related to the irregular timing of repetitive events sufficient to disrupt the sediment pile. Yet, such events remain relatively infrequent (9% of the core). Given the distance of the core site from fluvial inputs (2 to 26 km), it is unlikely that fluvial activity could generate sedimentation rapidly enough to produce relatively few but well-defined SSDS horizons. Instead, given the record of repeated (though infrequent) high-intensity earthquakes in the region, the simplest explanation for the sections of the core where SSDS are absent is that the pile accumulated for the most part via fine-grained fluvial inputs settling from suspension, only to be disrupted by singular high-energy events. If this argument is acceptable, then regional earthquakes are strongly implicated as the primary cause of the relatively infrequent disruptions. Given this scenario, we propose a model to explain the presence of SSDS observed in DX-2 (Fig. 11).

As noted in our introduction, a major impediment to interpreting SSDS genesis is that, as long as the SSDS remain unconsolidated, they are likely to experience multiple perturbations and overprinting of forms (Agnon et al. 2006; Alsop and Marco 2011; Molenaar et al. 2019, 2021). An upshot of rapid sedimentation rates like those at Diexi is that compaction and consolidation within the sediment pile evolve rapidly, such that only near-surface sediments will contain sufficient fluid to be ductile and fluidised by an earthquake. Sediment at depth would also experience shaking, but compacted sediment layers are more likely to have a brittle-fracture response to disturbance. In our conceptual model, only the surface sediments are repeatedly disrupted, forming SSDS each time an earthquake exceeds a certain threshold intensity. Micro-faulting (e.g., 2 mm thick; Fig. 9a) and the intrusion of dykes (< 9 mm in length) into otherwise ductile SSDS may occur due to strain-hardening during ductile flow, but can be explained more readily as a brittle overprint on SSDS that lie deeply buried, having attained a later stage of consolidation. Larger-scale faulting (e.g., 60 mm thick; Fig. 9b) and the presence of longer and thicker dykes (< 29 mm in length; Fig. 5c) intersecting SSDS may be attributed to earthquakes disrupting deeply buried and well-consolidated SSDS. Although it is reasonable to expect recent shallowly buried SSDS to be repeatedly disrupted by a sequence of two or more earthquakes, we did not find clear evidence in the structure of SSDS

for repeated disruption. We cannot rule out this overprint scenario completely, but assuming an average accumulation rate of 15 m per thousand years (Wang et al. 2012), SSDS will be buried by tens of metres after just a few millennia—a rate commensurate with the recurrence of high-intensity earthquakes. This conceptual model explains not only the relatively sparse distribution of SSDS up the core but also the presence of brittle fracture and larger dykes at depth within the core (Fig. 11).

We have compiled a list of 20 SSDS (Table 2), which previous workers have attributed to earthquakes of a given estimated intensity. Of these 20 SSDS types, the majority (17) are attributed to events of MMI equal to VI or greater, and the majority (13) are identified within the DX-2 core. In other words, the DX-2 core contains close to the full range of SSDS types associated with major earthquake events. Only four SSDS were not observed in the DX-2 core.

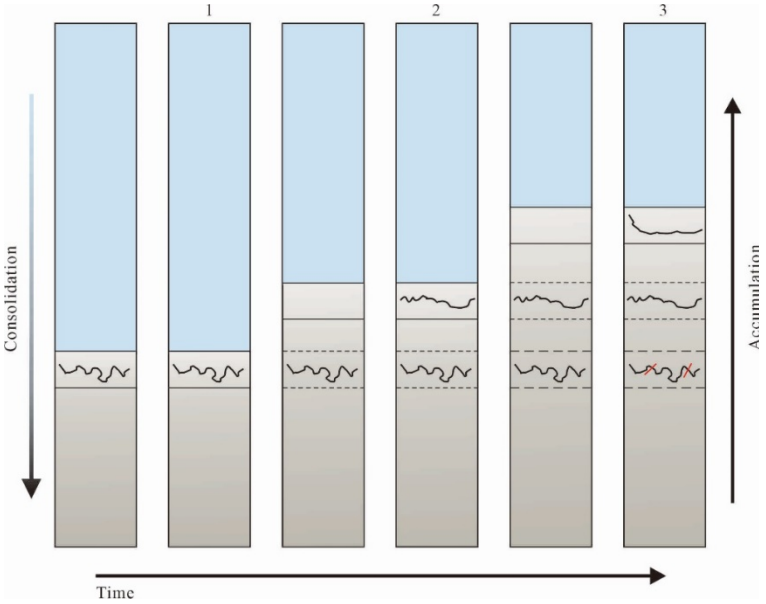

Fig. 11 Conceptual model of the development of SSDS within the Diexi palaeolake through time, depicting the general relationship between ductile (wiggly black lines) and brittle behaviour (short red lines) with progressive sediment consolidation down-core (including water column shown in blue).

6 Conclusions

We report a detailed sedimentological analysis of a ~166 m core (DX-2) extracted from the Diexi Palaeolake, eastern Tibetan Plateau. We describe and interpret 13 SSDS types: load structures (load casts, droplets, ball-pillow structures, injection structures), water escape structures (dish-and-pillar structures, pocket-and-pillar structures), sedimentary dykes, diapirs, breccias, plunged sediment mixtures, convolute laminations, slumps, and (stepped) micro-faults.

The Diexi Palaeolake is located in one of the most seismically active regions on Earth, which, when combined with extremely fast sedimentation rates (~15 mm/yr), makes this an outstanding site for studying SSDS. Although mass movement, rock avalanche-driven tsunamis, and rapid sedimentation are the possible triggering mechanisms, several lines of evidence support the hypothesis that earthquakes are the primary trigger mechanism for the SSDS observed in the DX-2 core: (1) different SSDS types are observed repeatedly in the long vertical sequence; (2) SSDS of similar ages are observed across the Diexi area; (3) several palaeoseismic events since 30 ka are identified in the upper Minjiang River; (4) large historical earthquakes (MMI > X, or M > 7) are documented and recorded in proximity to Diexi; and (5) controlled experiments demonstrate that seismic events can indeed trigger SSDS. We tentatively propose that the SSDS in the Diexi area are likely the product of earthquakes of MMI ≥ VI.

Acknowledgments

This research is financially supported by the National Natural Science Foundation for Distinguished Young Scholars of China (42125702), the National Natural Science Foundation for International Cooperation and Exchange (W2412050), the National Science and Technology Major Project of Sichuan Province (2024ZDZX0020), the New Cornerstone Science Foundation through the XPLORER PRIZE (XPLORER-2022-1012), the Activity Prediction and Risk Identification of Large-Scale Plateau Debris Flows (XZ202401ZY0029), and the Formation Mechanisms and Monitoring-Warning Methods for Moraine Soil Debris Flows in the Eastern Himalayan Syntaxis Region (XZ202401ZR0073). John Jansen acknowledges funding from the Czech Science Foundation (22-13190S), and Attila Çiner acknowledges a Humboldt Georg Forster grant for his

travel expenses. We thank WANG Ping and the team of LIU Fude, DAI Lanxin, ZOU Chengbin, LUO Binbin, RONG Zepeng, ZHONG Yujin, XIA Bing, and XIONG Kunyong for fieldwork assistance during the drilling of core DX-2, and DOU Xiangyang for improving the map of the Tibetan Plateau.

Author Contributions

LI Jingjuan: Conceptualization, investigation, methodology, validation, visualization, original draft, review & editing; JANSEN John D.: Methodology, supervision, validation, review & editing; CARLING Paul A.: Methodology, validation, visualization, review & editing; ÇINER Attila: Methodology, review & editing; FAN Xuanmei: Funding acquisition, investigation, project administration, resources, supervision, review & editing.

Ethics Declaration

Availability of Data/Materials: The data that support the findings of this study are available in the Supplementary file of this paper.

Conflict of Interest: The authors declare that they have no known competing financial interests or personal relationships that could have influenced the work reported in this paper.

Electronic Supplementary Material

Supplementary material (Appendixes 1-3) is available in the online version of this article at https://doi.org/10.1007/s11629-025-9874-y.

Open Access

Funding note: Open access publishing supported by the institutions participating in the CzechELib Transformative Agreement.

References

Agnon A, Migowski C, Marco S (2006) Intraclast breccias in laminated sequences reviewed: recorders of paleo-earthquakes. In: Enzel Y, Stein M, Agnon A (eds) New Frontiers in Dead Sea Paleoenvironmental Research. Geologiocal Society of America Special Paper, Boulder, Colorado. pp 195-214.

Alfaro P, Delgado J, Estévez A, et al. (2002) Liquefaction and fluidization structures in Messinian storm deposits (Bajo Segura Basin, Betic Cordillera, southern Spain). Int J Earth Sci 91:505-513. https://doi.org/10.1007/s00531-001-0241-z

Alfaro P, Moretti M, Soria MJ (1997) Soft sediment deformation structures induced by earthquakes (seismites) in Pliocene lacustrine deposits (Guadix-Baza Basin, central Betic Cordillera). Eclogae Geol Helv 90:531-540.

Allen JRL (1977) The possible mechanics of convolute lamination in graded sand beds. J Geol Soc 134:19-31. https://doi.org/10.1144/gsjgs.134.1.0019

Allen JRL (1982) Sedimentary structures: their character and physical basis. Amsterdam: Elsevier.

Allen JRL (1986) Earthquake magnitude-frequency, epicentral distance, and soft-sediment deformation in sedimentary basins. Sediment Geol 46:67-75. https://doi.org/10.1016/0037-0738(86)90006-0

Alsop GI, Marco S (2011) Soft-sediment deformation within seismogenic slumps of the Dead Sea Basin. J Struct Geol 33:433-457. https://doi.org/10.1016/j.jsg.2011.02.003

Alsop GI, Marco S (2013) Seismogenic slump folds formed by gravity-driven tectonics down a negligible subaqueous slope. Tectonophysics 605:48-69. https://doi.org/10.1016/j.tecto.2013.04.004

Ambraseys NN (1988) Engineering seismology. Earthquake Eng Struct Dyn 17:1-105. https://doi.org/10.1002/eqe.4290170101

Anketell JM, Cegla J, Dzulinsky S (1970) On the deformational structures in systems with reverse density gradients. Annales dela Societe Geologique de Pologne XL (1):3-30.

Atkinson GM, Finn L, Charlwood RG (1984) Simple computation of liquefaction probability for seismic hazard applications. Earthq Spectra 1:107-123. https://doi.org/10.1193/1.1585259

Audemard FA, Santis Fd (1991) Survey of liquefaction structures induced by recent moderate earthquakes. Bulletin of Engineering Geology and the Environment 44:5-16. https://doi.org/10.1007/BF02602705

Azennoud K, Baali A, El Asmi H, et al. (2022) Soft-sediment deformation structures recognised in a reverse-drag associated with normal faulting (Lake Ifrah, northwest Africa): palaeoseismic assessment and neotectonic implications. Sediment Geol 441:1-26. https://doi.org/10.1016/j.sedgeo.2022.106264

Berra F, Felletti F (2011) Syndepositional tectonics recorded by soft-sediment deformation and liquefaction structures (continental Lower Permian sediments, Southern Alps, Northern Italy): Stratigraphic significance. Sediment Geol 235:249-263. https://doi.org/10.1016/j.sedgeo.2010.08.006

Bertran P, Font M, Giret A, et al. (2019) Experimental soft-sediment deformation caused by fluidization and intrusive ice melt in sand. Sedimentology 66:1102-1117. https://doi.org/10.1111/sed.12537

Bhadran A, Duarah BP, Girishbai D, et al. (2023) Soft sediment deformation structures from the Brahmaputra Basin: a window to the eastern Himalayan paleoseismicity and tectonics. J Asian Earth Sci 259:1-13. https://doi.org/10.1016/j.jseaes.2023.105894

Brandes C, Winsemann J (2013) Soft-sediment deformation structures in NW Germany caused by late Pleistocene seismicity.

Int J Earth Sci 102:2255-2274. https://doi.org/10.1007/s00531-013-0914-4
Brenchley PJ, Newall G (1977) The significance of contorted bedding in the Upper Ordovician sediments of the Oslo region, Norway. J Sediment Petrol 47:819-833. https://doi.org/10.1306/212f7261-2b24-11d7-8648000102c1865d
Calvo JP, Rodriguez-Pascua M, Martin-Velazquez S, et al. (1998) Microdeformation of lacustrine laminite sequences from late Miocene formations of SE Spain: an interpretation of loop bedding. Sedimentology 45:279-292. https://doi.org/10.1046/j.1365-3091.1998.00145.x
Chai HJ, Liu HC (2002) Study on landslide damming of river in upper of Minjiang River. J Mt Sci 20:616-620. (In Chinese)
Chai HJ, Liu HC, Zhang ZY (1995) Time catalogue of China's landslide blocking the river. Geol Hazards Environ Prot 6:1-9. (In Chinese)
Chakraborty PP, Sharma R, Kumar P (2019) Earthquake-induced soft sediment deformation (SSD) structures from the Bilara limestone formation, Marwar Basin, India. J Earth Syst Sci 128:1-16. https://doi.org/10.1007/s12040-019-1182-x
Chen GG, Ji FJ, Zhou RJ, et al. (2007) Primary research of activity segmentation of Longmenshan Fault zone since late-Quaternary. Seismol Geol 29:657-673. (In Chinese)
Chen JT, Lee HS (2013) Soft-sediment deformation structures in Cambrian siliciclastic and carbonate storm deposits (Shandong Province, China): differential liquefaction and fluidization triggered by storm-wave loading. Sediment Geol 288:81-94. https://doi.org/10.1016/j.sedgeo.2013.02.001
Chen ZE, Lin QY (1993) Significance of neotectonic movement of lake extension and shrinkage in Qinghai-Tibet Plateau. Earthquake:31-40+52. (In Chinese)
Dai LX, Fan XM, Jansen JD, et al. (2021) Landslides and fluvial response to landsliding induced by the 1933 Diexi earthquake, Minjiang River, eastern Tibetan Plateau. Landslides 18:3011-3025. https://doi.org/10.1007/s10346-021-01717-2
Dai LX, Fan XM, Wang D, et al. (2023) Electrical resistivity tomography revealing possible breaching mechanism of a late Pleistocene long-lasted gigantic rockslide dam in Diexi, China. Landslides 20:1449-1463. https://doi.org/10.1007/s10346-023-02048-0
Deev E, Turova I, Borodovskiy A, et al. (2019) Large earthquakes in the Katun Fault zone (Gorny Altai): paleoseismological and archaeoseismological evidence. Quat Sci Rev 203:68-89. https://doi.org/10.1016/j.quascirev.2018.11.009
Deng B, Liu SG, Liu S, et al. (2013) Progressive Indosinian N-S deformation of the Jiaochang structure in the Songpan-Ganzi fold-belt, western China. PLoS One 8:e76732. https://doi.org/10.1371/journal.pone.0076732
Deng QD, Chen SF, Zhao XL (1994) Tectonics, seismicity and dynamics of Longmenshan mountains and its adjacent regions. Seismol Geol 16:389-430. (In Chinese)
Densmore AL, Ellis MA, Li Y, et al. (2007) Active tectonics of the Beichuan and Pengguan Faults at the eastern margin of the Tibetan Plateau. Tectonics 26:1-17. https://doi.org/10.1029/2006tc001987
Druguet E, Alsop GI, Carreras J (2009) Coeval brittle and ductile structures associated with extreme deformation partitioning in a multilayer sequence. J Struct Geol 31:498-511. https://doi.org/10.1016/j.jsg.2009.03.004
Ettensohn FR, Zhang C, Gao L, et al. (2011) Soft-sediment deformation in epicontinental carbonates as evidence of paleoseismicity with evidence for a possible new seismogenic indicator: Accordion folds. Sediment Geol 235:222-233. https://doi.org/10.1016/j.sedgeo.2010.09.022
Ezquerro L, Moretti M, Liesa CL, et al. (2016) Controls on space-time distribution of soft-sediment deformation structures: applying palaeomagnetic dating to approach the apparent recurrence period of paleoseisms at the Concud Fault (eastern Spain). Sediment Geol 344:91-111. https://doi.org/10.1016/j.sedgeo.2016.06.007
Ezquerro L, Moretti M, Liesa CL, et al. (2015) Seismites from a well core of palustrine deposits as a tool for reconstructing the palaeoseismic history of a fault. Tectonophysics 655:191-205. https://doi.org/10.1016/j.tecto.2015.05.025
Fan C, Wang EQ, Wang G, et al. (2008) Dextral strike-slip and tectonic transformation of the northern Longmen Shan fault belt from late Neogene: a case study from the Qingchuan Fault. Chin J Geol 43:417-433. (In Chinese)
Fan XM, Dai LX, Zhong YJ, et al. (2021) Recent research on the Diexi paleo-landslide: dam and lacustrine deposits upstream of the Minjiang River, Sichuan, China. Earth Sci Front 28:71-84. (In Chinese)
Fan XM, Scaringi G, Korup O, et al. (2019) Earthquake-induced chains of geologic hazards: patterns, mechanisms, and impacts. Rev Geophys 57:421-503.https://doi.org/10.1029/2018rg000626
Fan XM, Scaringi G, Xu Q, et al. (2018) Coseismic landslides triggered by the 8th August 2017 Ms 7.0 Jiuzhaigou earthquake (Sichuan, China): Factors controlling their spatial distribution and implications for the seismogenic blind fault identification. Landslides 15:967-983. https://doi.org/10.1007/s10346-018-0960-x
Fan XM, Xu Q, Van Westen CJ, et al. (2017) Characteristics and classification of landslide dams associated with the 2008 Wenchuan earthquake. Geoenvironmental Disasters 4:1-15. https://doi.org/10.1186/s40677-017-0079-8
Fan XM, Yunus AP, Jansen JD, et al. (2022) Comment on 'Gigantic rockslides induced by fluvial incision in the Diexi area along the eastern margin of the Tibetan Plateau' by Zhao et al. (2019) Geomorphology 338, 27-42. Geomorphology 402:1-8. https://doi.org/10.1016/j.geomorph.2019.106963
Field ME, Gardner JV, Jennings AE, et al. (1982) Earthquake-induced sediment failures on a 0.25° slope, Klamath River delta, California. Geology 10:542-546. https://doi.org/10.1130/0091-7613(1982)10<542:ESFOAS>2.0.CO;2
Franco A, Moernaut J, Schneider-Muntau B, et al. (2020) The 1958 Lituya Bay tsunami-pre-event bathymetry reconstruction and 3D numerical modelling utilising the computational fluid dynamics software Flow-3D. Nat Hazards Earth Syst Sci 20:2255-2279. https://doi.org/10.5194/nhess-20-2255-2020
Fu JD, Ren JW, Zhang JL, et al. (2012) Research on late Quaternary paleoearthquake on Tazang Fault on the eastern section of the Kunlun active fault. Quat Sci 32:473-483. (In Chinese)
García-Tortosa FJ, Alfaro P, Gibert L, et al. (2011) Seismically induced slump on an extremely gentle slope (<1°) of the Pleistocene Tecopa paleolake (California). Geology 39:1055-1058. https://doi.org/10.1130/g32218.1
Ghosh SK, Pandey AK, Pandey P, et al. (2012) Soft-sediment deformation structures from the Paleoproterozoic Damtha Group of Garhwal Lesser Himalaya, India. Sediment Geol 261-262:76-89. https://doi.org/10.1016/j.sedgeo.2012.03.006
Gibert L, Alfaro P, García-Tortosa FJ, et al. (2011) Superposed deformed beds produced by single earthquakes (Tecopa Basin, California): insights into paleoseismology. Sediment Geol 235:148-159. https://doi.org/10.1016/j.sedgeo.2010.08.003
Gilli A, Anselmetti FS, Glur L, et al. (2013) Lake sediments as archives of recurrence rates and intensities of past flood events. In: Schneuwly-Bollschweiler M, Stoffel M, Florian R-MR-M (eds.) Dating torrential processes on Fans and Cones. Springer, Berlin. p 225-242.
Gladkov AS, Lobova EU, Deev EV, et al. (2016) Earthquake-induced soft-sediment deformation structures in late Pleistocene lacustrine deposits of Issyk-Kul Lake (Kyrgyzstan). Sediment Geol 344:112-122. https://doi.org/10.1016/j.sedgeo.2016.06.019
Gladstone C, McClelland HLO, Woodcock NH, et al. (2018) The formation of convolute lamination in mud-rich turbidites. Sedimentology 65:1800-1825. https://doi.org/10.1111/sed.12447
Gorum T, Fan XM, Van Westen CJ, et al. (2011) Distribution pattern of earthquake-induced landslides triggered by the 12 May 2008 Wenchuan earthquake. Geomorphology 133:152-167. https://doi.org/10.1016/j.geomorph.2010.12.030
Greb SF, Archer AW (2007) Soft-sediment deformation produced by tides in a meizoseismic area, Turnagain Arm, Alaska. Geology 35:435-438. https://doi.org/10.1130/g23209a.1

Gu GX (1983) Catalogue of earthquakes in China. Beijing: Science Press.
Guo P (2018) Grain size characteristics and optically stimulated luminescence geochronology of sediments in Diexi palaeo-dammed Lake, upper reaches of Minjiang River. Master thesis, China University of Geosciences, Beijing. p 85. (In Chinese)
Harazim D, Callow RHT, McIlroy D, et al. (2013) Microbial mats implicated in the generation of intrastratal shrinkage ('synaeresis') cracks. Sedimentology 60:1621-1638. https://doi.org/10.1111/sed.12044
Hart JK, Boulton GS (1991) The interrelation of glaciotectonic and glaciodepositional processes within the glacial environment. Quaternary Science Rewews 10:335-350. https://doi.org/10.1016/0277-3791(91)90035-S
He BZ, Jiao CL, Xu ZQ, et al. (2011) Manifestation of the Middle-Late Caledonian tectonic movement along the Altun-West Kunlun orogenic belt in the Tangguzibas depression, Tarim Basin. Acta Petrol Sin 27:3435-3448. (In Chinese)
Hilbert-Wolf HL, Simpson EL, Simpson WS, et al. (2009) Insights into syndepositional fault movement in a foreland basin; trends in seismites of the Upper Cretaceous, Wahweap Formation, Kaiparowits Basin, Utah, USA. Basin Res 21:856-871. https://doi.org/10.1111/j.1365-2117.2009.00398.x
Holzer TL, Hanks TC, Youd TL (1989) Dynamics of liquefaction during the 1987 Superstition Hills California, earthquake. Science 244:56-59.
Hou ZQ, Li ZQ, Qu XM, et al. (2001) The uplift process of the Qinghai-Tibet Plateau since 0.5 Ma–Evidence from hot water activity in the Gangdese belt. Sci China 31:27-33. (In Chinese)
Huang XN, Yang XP, Hu ZK, et al. (2023) Characteristics of the late-Quaternary activity of the western segment of Bailongjiang Fault. Technol Earthquake Disaster Prev 18:701-717. (In Chinese)
Huang ZZ, Tang RC, Liu SL (2003) Re-discussion on the Jiaochang arcuate structure, Sichuan Province, and the seismogenic structure for Diexi earthquake in 1933. Earthquake Res China 17:51-62.
Jiang HC, Mao X, Xu HY, et al. (2014) Provenance and earthquake signature of the last deglacial Xinmocun lacustrine sediments at Diexi, east Tibet. Geomorphology 204:518-531. https://doi.org/10.1016/j.geomorph.2013.08.032
Jiang HC, Zhong N, Li YH, et al. (2016) Soft sediment deformation structures in the Lixian lacustrine sediments, eastern Tibetan Plateau and implications for postglacial seismic activity. Sediment Geol 344:123-134. https://doi.org/10.1016/j.sedgeo.2016.06.011
Jiang WL, Han ZJ, Guo P, et al. (2017) Slip rate and recurrence intervals of the east Lenglongling Fault constrained by morphotectonics: tectonic implications for the northeastern Tibetan Plateau. Lithosphere 9:417-430. https://doi.org/10.1130/l597.1
Jones AP, Omoto K (2000) Towards establishing criteria for identifying trigger mechanisms for soft-sediment deformation: a case study of late Pleistocene lacustrine sands and clays, Onikobe and Nakayamadaira Basins, northeastern Japan. Sedimentology 47:1211-1226. https://doi.org/10.1046/j.1365-3091.2000.00355.x
Kahle CF (2002) Seismogenic deformation structures in microbialites and mudstones, silurian lockport dolomite, northwestern Ohio, U.S.A. J Sediment Res 72:201-216. https://doi.org/10.1306/051501720201
Kiefer C, Oswald P, Moernaut J, et al. (2021) A 4,000 year debris-flow record based on amphibious investigations of fan delta activity in Plansee (Austria, eastern Alps). Earth Surf Dyn 23:1-27. https://doi.org/10.5194/esurf-2021-23
Ko KT, Kim SW, Lee HJ, et al. (2017) Soft sediment deformation structures in a lacustrine sedimentary succession induced by volcano-tectonic activities: an example from the Cretaceous Beolgeumri Formation, Wido Volcanics, Korea. Sediment Geol 358:197-209. https://doi.org/10.1016/j.sedgeo.2017.07.008
Koç Taşgın C (2011) Seismically-generated hydroplastic deformation structures in the late Miocene lacustrine deposits of the Malatya Basin, eastern Turkey. Sediment Geol 235:264-276. https://doi.org/10.1016/j.sedgeo.2010.09.015
Koç Taşgın C, Orhan H, Türkmen İ, et al. (2011) Soft-sediment deformation structures in the late Miocene Şelmo Formation around Adıyaman area, southeastern Turkey. Sediment Geol 235:277-291. https://doi.org/10.1016/j.sedgeo.2010.08.005
Komatsubara J, Fujiwara O, Takada K, et al. (2008) Historical tsunamis and storms recorded in a coastal lowland, Shizuoka Prefecture, along the Pacific Coast of Japan. Sedimentology 55:1703-1716. https://doi.org/10.1111/j.1365-3091.2008.00964.x
Kremer K, Hilbe M, Simpson G, et al. (2015) Reconstructing 4000 years of mass movement and tsunami history in a deep peri-Alpine lake (Lake Geneva, France-Switzerland). Sedimentology 62:1305-1327. https://doi.org/10.1111/sed.12190
Kuenen PH (1958) Experiments in geology. Trans Geol Soc Glasg 23:1-28. https://doi.org/10.1144/transglas.23.centenary.1
Le Heron DP, Etienne JL (2005) A complex subglacial clastic dyke swarm, Sólheimajökull, southern Iceland. Sediment Geol 181:25-37. https://doi.org/10.1016/j.sedgeo.2005.06.012
Le Roux JP, Nielsen SN, Kemnitz H, et al. (2008) A Pliocene mega-tsunami deposit and associated features in the Ranquil Formation, southern Chile. Sediment Geol 203:164-180. https://doi.org/10.1016/j.sedgeo.2007.12.002
Lee JR, Phillips ER (2008) Progressive soft sediment deformation within a subglacial shear zone-a hybrid mosaic-pervasive deformation model for middle Pleistocene glaciotectonised sediments from eastern England. Quat Sci Rev 27:1350-1362. https://doi.org/10.1016/j.quascirev.2008.03.009
Li CS, Wu YS, Li YZ (1964) The Quaternary glacier historic relic of the Longmen Mountain south segment east brae in Sichuan Province. In: Research CAfQ (eds.), The Chinese Quaternary Glacier historic relic research collection of Corpu.Science Publisher, Beijing. p 14-86.
Li CX (2009) The long-term faulting behavior of the eastern segment (Maqin-Maqu) of the east Kunlun Fault since the late Quaternary. PhD degree, Institute of Geology, China Earthquake Administration, Beijing. p (In Chinese)
Li CX, Yuan DY, Yang H, et al. (2016) The tectonic activity characteristics of Awancang Fault in the Late Quaternary, the sub-strand of the eastern Kunlun Fault. Seismol Geol 38:44-64. (In Chinese)
Li F, Liu HG, Jia QC, et al. (2018) Holocene active characteristics of the northern segment of the Minjiang Fault in the eastern margin of the Tibetan Plateau. Seismol Geol 40:97-106. (In Chinese)
Li JJ, Fang XM (1998) Study on the uplift and environmental change of the Qinghai-Tibet Plateau. Chin Sci Bull 43:1563-1574. (In Chinese)
Li JJ, Jansen JD, Fan XM, et al. (2024) Terrace formation linked to outburst floods at the Diexi palaeo-landslide dam, upper Minjiang River, eastern Tibetan Plateau. Earth Surf Dyn 12:953-971. https://doi.org/10.5194/esurf-12-953-2024
Lin AM, Fu BH, Guo JM, et al. (2002) Co-seismic strike-slip and rupture length produced by the 2001 Ms 8.1 central Kunlun earthquake. Science 296:2015-2017. https://doi.org/10.1126/science.1070879
Lowe DR (1975) Water escape structures in coarse-grained sediments. Sedimentology 22:157-204. https://doi.org/10.1111/j.1365-3091.1975.tb00290.x
Lowe DR, Lopiccolo RD (1974) The characteristics and origins of dish and pillar structures. J Sediment Petrol 44:484-501. https://doi.org/10.1306/74D72A68-2B21-11D7-8648000102C1865D
Lu HY, An ZS, Wang XY, et al. (2004) The staged uplift of the northeastern margin of the Qinghai-Tibet Plateau in the recent 14 Ma geomorphic evidence. Science in China Series D Earth Sciences 34:855-864. (In Chinese)
Ma JX (2017) Sedimentary characteristics of outburst deposits and inversion of outburst flood induced by the Diexi paleo dammed Lake of the upper Minjiang River in China. Master degree, China University of Geosciences, Beijing. p 97. (In Chinese)
Mao X (2011) Preliminary study on lacustrine sediments at Diexi in the upper reach of the Minjiang River during the last deglaciation. Master degree, China University of Geosciences, Beijing. p 71. (In Chinese)
Marco S, Agnon A (1995) Prehistoric earthquake deformations near Masada, Dead Sea graben. Geology 23:695-698.

https://doi.org/10.1130/0091-7613(1995)023<0695:PEDNMD>2.3.CO;2
Massari F, Ghibaudo G, D'Alessandro A, et al. (2001) Water-upwelling pipes and soft-sediment-deformation structures in lower Pleistocene calcarenites (Salento, southern Italy). Geol Soc Am Bull 113:545-560. https://doi.org/10.1130/0016-7606(2001)113<0545:WUPASS>2.0.CO;2
McLaughlin PI, Brett CE (2004) Eustatic and tectonic control on the distribution of marine seismites: examples from the Upper Ordovician of Kentucky, USA. Sediment Geol 168:165-192. https://doi.org/10.1016/j.sedgeo.2004.02.005
Miall AD (2000) Principles of sedimentary basin. Berlin: Springer.
Middleton GV, Church MJ, Coniglio M, et al. (2003) Encyclopedia of sediments and sedimentary rocks. London: Kluwer Academic Publishers.
Miller DJ (1960) Giant waves in Lituya Bay, Alaska Washington: Survey USG.
Mills PC (1983) Genesis and diagnostic value of soft sediment deformation structures-a review. Sediment Geol 35:83-104. https://doi.org/10.1016/0037-0738(83)90046-5
Mohindra R, Bagati TN (1996) Seismically induced soft-sediment deformation structures (seismites) around Sumdo in the lower Spiti Valley (Tethys Himalaya). Sediment Geol 101:69-83. https://doi.org/10.1016/0037-0738(95)00022-4
Molenaar A, Moernaut J, Wiemer G, et al. (2019) Earthquake impact on active margins: tracing surficial remobilization and seismic strengthening in a slope sedimentary sequence. Geophys Res Lett 46:6015-6023. https://doi.org/10.1029/2019gl082350
Molenaar A, Van Daele M, Vandorpe T, et al. (2021) What controls the remobilization and deformation of surficial sediment by seismic shaking? Linking lacustrine slope stratigraphy to great earthquakes in South-Central Chile. Sedimentology 68:2365-2396. https://doi.org/10.1002/essoar.10504161.1
Molenaar A, Wils K, Van Daele M, et al. (2024) Shaken and stirred: a comparative study of earthquake-triggered soft-sediment deformation structures in lake sediments. Geochemistry, Geophysics, Geosystems 25:1-18. https://doi.org/10.1029/2023gc011402
Monecke K, Anselmetti FS, Becker A, et al. (2007) Earthquake-induced deformation structures in lake deposits: a late Pleistocene to Holocene paleoseismic record for central Switzerland. Eclogae Geol Helv 99. https://doi.org/10.1007/s00015-006-1193-x
Monecke K, Anselmetti FS, Becker A, et al. (2004) The record of historic earthquakes in lake sediments of central Switzerland. Tectonophysics 394. https://doi.org/10.1016/j.tecto.2004.07.053
Montenat C, Barrier P, Ott d'Estevou P, et al. (2007) Seismites: an attempt at critical analysis and classification. Sediment Geol 196:5-30. https://doi.org/10.1016/j.sedgeo.2006.08.004
Moretti M (2000) Soft-sediment deformation structures interpreted as seismites in middle-late Pleistocene aeolian deposits (Apulian foreland, southern Italy). Sediment Geol 135:167-179. https://doi.org/10.1016/S0037-0738(00)00070-1
Moretti M, Alfaro P, Caselles O, et al. (1999) Modelling seismites with a digital shaking table. Tectonophysics 304:369-383. https://doi.org/10.1016/s0040-1951(98)00289-3
Moretti M, Pieri P, Tropeano M (2002) Late Pleistocene soft-sediment deformation structure interpreted as seismites in paralic deposits in the city of Bari (Apulian Foreland, southern Italy). In: Ettensohn FR, Rast N, Brett CE (eds) Ancient seismites. Geological Society of America Special Paper, Boulder, Colorado. p 75-85.
Moretti M, Sabato L (2007) Recognition of trigger mechanisms for soft-sediment deformation in the Pleistocene lacustrine deposits of the Sant'Arcangelo Basin (Southern Italy): seismic shock vs. overloading. Sediment Geol 196:31-45. https://doi.org/10.1016/j.sedgeo.2006.05.012
Moretti M, Soria JM, Alfaro P, et al. (2001) Asymmetrical soft-sediment deformation structures triggered by rapid sedimentation in turbiditic deposits. Facies 44:283-294. https://doi.org/10.1007/BF02668179
Moretti M, Van Loon AJ (2014) Restrictions to the application of 'diagnostic' criteria for recognizing ancient seismites. J Palaeogeogr 3. https://doi.org/10.3724/SP.J.1261.2014.00050
Morton RA, Gelfenbaum G, Jaffe BE (2007) Physical criteria for distinguishing sandy tsunami and storm deposits using modern examples. Sediment Geol 200:184-207. https://doi.org/10.1016/j.sedgeo.2007.01.003
Moura-Lima EN, Bezerra FHR, Lima-Filho FP, et al. (2011) 3-D geometry and luminescence chronology of Quaternary soft-sediment deformation structures in gravels, northeastern Brazil. Sediment Geol 235:160-171. https://doi.org/10.1016/j.sedgeo.2010.09.016
Mulder T, Cochonat P (1996) Classification of offshore mass movements. J Sediment Res 66:43-57. https://doi.org/10.1306/D42682AC-2B26-11D7-8648000102C1865D
Müller K, Winsemann J, Pisarska-Jamroży M, et al. (2021) The challenge to distinguish soft-sediment deformation structures (SSDS) formed by glaciotectonic, periglacial and seismic processes in a formerly glaciated area: a review and synthesis. In: Steffen H, Olesen O, Sutinen R (eds) Glacially-Triggered Faulting. Cambridge University Press, Cambridge. p 67-88.
Myrow PM, Southard JB (1996) Tempestite deposition. J Sediment Res 66:875-887. https://doi.org/10.1306/D426842D-2B26-11D7-8648000102C1865D
Nanayama F, Shigeno K, Satake K, et al. (2000) Sedimentary differences between the 1993 Hokkaido-nansei-oki tsunami and the 1959 Miyakojima typhoon at Taisei, southwestern Hokkaido, northern Japan. Sediment Geol 135:255-264. https://doi.org/10.1016/s0037-0738(00)00076-2
Neuwerth R, Suter F, Guzman CA, et al. (2006) Soft-sediment deformation in a tectonically active area: the Plio-Pleistocene Zarzal Formation in the Cauca Valley (western Colombia). Sediment Geol 186:67-88. https://doi.org/10.1016/j.sedgeo.2005.10.009
Obermeier SF (1996) Use of liquefaction-induced features for paleoseismic analysis-an overview of how seismic liquefaction features can be distinguished from other features and how their regional distribution and properties of source sediment can be used to infer the location and strength of Holocene paleo-earthquakes. Eng Geol 44:1-76. https://doi.org/10.1016/S0013-7952(96)00040-3
Obermeier SF, Jacobson RB, Smoot JP, et al. (1990) Earthquake-induced liquefaction features in the coastal setting of south Carolina and in the fluvial setting of the New Madrid seismic zone. U S Geol Surv Prof Pap 1504:1-44. https://doi.org/10.3133/pp1504
Onorato MR, Perucca L, Coronato A, et al. (2016) Seismically-induced soft-sediment deformation structures associated with the Magallanes–Fagnano Fault System (Isla Grande de Tierra del Fuego, Argentina). Sediment Geol 344:135-144. https://doi.org/10.1016/j.sedgeo.2016.04.010
Owen G (1987) Deformation processes in unconsolidated sands. London: Deformation processes in unconsolidated sands.
Owen G (1995) Soft-sediment deformation in Upper Proterozoic Torridonian Sandstones (Applecross Formation) at Torridon, northwest Scotland. J Sediment Res A65:495-504. https://doi.org/10.1306/D4268108-2B26-11D7-8648000102C1865D
Owen G (1996) Experimental soft-sediment deformation: structures formed by the liquefaction of unconsolidated sands and some ancient examples. Sedimentology 43:279-193. https://doi.org/10.1046/j.1365-3091.1996.d01-5.x
Owen G (2003) Load structures: gravity-driven sediment mobilization in the shallow subsurface. London: Geological Society of London.
Owen G, Moretti M (2011) Identifying triggers for liquefaction-induced soft-sediment deformation in sands. Sediment Geol 235:141-147. https://doi.org/10.1016/j.sedgeo.2010.10.003
Owen G, Moretti M, Alfaro P (2011) Recognising triggers for soft-sediment deformation: current understanding and future directions. Sediment Geol 235:133-140. https://doi.org/10.1016/j.sedgeo.2010.12.010

Pandey P, Kumar R, Suresh N, et al. (2009) Soft-sediment deformation in contemporary reservoir sediment: a repository of recent major earthquake events in Garhwal Himalaya. J Geol 117:200-209. https://doi.org/10.1086/595860
Panja M, Chakrabarti G, Shome D (2018) Earthquake induced soft sediment deformation structures in the Paleoproterozoic Vempalle Formation (Cuddapah Basin, India). Carbonates Evaporites 34. https://doi.org/10.1007/s13146-017-0412-z
Picard MD, High LR (1972) Paleoenvironmental reconstructions in an area of rapid facies change, Parachute Creek Member of Green River Formation (Eocene), Uinta Basin, Utah. Geol Soc Am Bull 83:2689-2708. https://doi.org/10.1130/0016-7606(1972)83[2689:PRIAAO]2.0.CO;2
Purvis K, Kao J, Flanagan K, et al. (2002) Complex reservoir geometries in a deep water clastic sequence, Gryphon Field, UKCS: injection structures, geological modelling and reservoir simulation. Mar Pet Geol 19:161-179. https://doi.org/10.1016/s0264-8172(02)00003-x
Qiao XF, Guo XP (2011) On the Lower Jurassic soft-sediment deformation of southwestern Tianshan Mountains, Xinjiang, China. Geol Rev 57:761-769. (In Chinese)
Qiao XF, Li HB (2008) Seismic event, sequence and tectonic significance in Canglangpu Stage in Paleo-Tanlu Fault Zone. Geol Rev 54:721-730. (In Chinese)
Rana N, Bhattacharya F, Basavaiah N, et al. (2013) Soft sediment deformation structures and their implications for late Quaternary seismicity on the south Tibetan Detachment System, central Himalaya (Uttarakhand), India. Tectonophysics 592:165-174. https://doi.org/10.1016/j.tecto.2013.02.020
Rana N, Sati SP, Sundriyal Y, et al. (2016) Genesis and implication of soft-sediment deformation structures in high-energy fluvial deposits of the Alaknanda Valley, Garhwal Himalaya, India. Sediment Geol 344:263-276. https://doi.org/10.1016/j.sedgeo.2016.06.012
Ren JJ, Xu XW, Yeats RS, et al. (2013) Latest Quaternary paleoseismology and slip rates of the Longriba Fault zone, eastern Tibet: implications for fault behavior and strain partitioning. Tectonics 32:216-238. https://doi.org/10.1002/tect.20029
Ren JJ, Xu XW, Zhang SM, et al. (2018) Surface rupture of the 1933 M 7.5 Diexi earthquake in eastern Tibet: implications for seismogenic tectonics. Geophys J Int 212:1627-1644. https://doi.org/10.1093/gji/ggx498
Rodríguez-Pascua MA, Calvo JP, Vicente GD, et al. (2000) Soft-sediment deformation structures interpreted as seismites in lacustrine sediments of the Prebetic Zone, SE Spain, and their potential use as indicators of earthquake magnitudes during the late Miocene. Sediment Geol 135:117-135. https://doi.org/10.1016/S0037-0738(00)00067-1
Rodríguez-Pascua MA, Garduño-Monroy VH, Israde-Alcántara I, et al. (2010) Estimation of the paleoepicentral area from the spatial gradient of deformation in lacustrine seismites (Tierras Blancas Basin, Mexico). Quat Int 219:66-78. https://doi.org/10.1016/j.quaint.2009.11.006
Rossetti DF (1999) Soft-sediment deformation structures in late Albian to Cenomanian deposits, São Luís Basin, northern Brazil: evidence for palaeoseismicity. Sedimentology 46:1065-1081. https://doi.org/10.1046/j.1365-3091.1999.00265.x
Rossetti DF, Bezerra FHR, Góes AM, et al. (2011) Sediment deformation in Miocene and post-Miocene strata, northeastern Brazil: evidence for paleoseismicity in a passive margin. Sediment Geol 235:172-187.https://doi.org/10.1016/j.sedgeo.2010.02.005
Rossetti DF, Góes AM (2000) Deciphering the sedimentological imprint of paleoseismic events: an example from the Aptian Codo Formation, northern Brazil. Sediment Geol 135:137-156. https://doi.org/10.1016/S0037-0738(00)00068-3
Schnellmann M, Anselmetti FS, Giardini D, et al. (2007) 15,000 Years of mass-movement history in Lake Lucerne: implications for seismic and tsunami hazards. Eclogae Geol Helv 99:409-428. https://doi.org/10.1007/s00015-006-1196-7
Seilacher A (1969) Fault-graded beds interpreted as seismites. Sedimentology 13:155-159. https://doi.org/10.1111/j.1365-3091.1969.tb01125.x
Shanmugam G (2016) The seismite problem. J Palaeogeogr 5:318-362. https://doi.org/10.1016/j.jop.2016.06.002
Shen M (2014) Earthquake information study for paleo-dammed lake at Minjiang River Upstream. Master thesis, Chengdu University of Technology, Chengdu. p 1-129. (In Chinese)
Shi W, Jiang HC, Alsop GI, et al. (2022) A continuous 13.3-ka paleoseismic record constrains major earthquake recurrence in the Longmen Shan Collision Zone. Front Earth Sci 10. https://doi.org/10.3389/feart.2022.838299
Shi YF, Li JJ, Li BY, et al. (1999) Uplift of the Qinghai—Xizang (Tibetan) Plateau and east Asia environmental change during late cenozoic. Acta Geogr Sin 54:12-22. (In Chinese)
Sieh KE (1978) Prehistoric large earthquakes produced by slip on the San Andreas Fault at Pallett Creek, California. J Geophys Res 83:3907-3939. https://doi.org/10.1029/JB083iB08p03907
Sims JD (1973) Earthquake-reduced structures in sediments of Van Norman Lake, San Fernando, California. Science 182:161-163. https://doi.org/10.1126/science.182.4108.161
Sims JD (1975) Determining earthquake recurrence intervals from deformational structures in young lacustrine sediments. Tectonophysics 28:141-152. https://doi.org/10.1016/B978-0-444-41420-5.50020-4
Staley SE, Fawcett PJ, Anderson RS, et al. (2021) Early Pleistocene-to-present paleoclimate archive for the American Southwest from Stoneman Lake, Arizona, USA. GSA Bull 134:791-814. https://doi.org/10.1130/b36038.1
Stauffer PH (1965) Sedimentation of lower Tertiary marine deposits, Santo Ynez Mountains, California. PhD thesis, Stanford University, Palo Alto. p 200.
Stauffer PH (1967) Grain-flow deposits and their implications, Santa Ynez Mountains, California. J Sediment Petrol 37:487-508. https://doi.org/10.1306/74D716F9-2B21-11D7-8648000102C1865D
Strunk A, Olsen J, Sanei H, et al. (2020) Improving the reliability of bulk sediment radiocarbon dating. Quat Sci Rev 242. https://doi.org/10.1016/j.quascirev.2020.106442
Sun HY (2015) Late Quaternary activity of the Qingchuan fault: Implications for the tectonic movement mechanism in regional area. PhD thesis, Institute of Geology, China Earthquake Administration, Beijing. p 1-116. (In Chinese)
Suter F, Martínez JI, Vélez MI (2011) Holocene soft-sediment deformation of the Santa Fe-Sopetrán Basin, northern Colombian Andes: evidence for pre-Hispanic seismic activity? Sediment Geol 235:188-199. https://doi.org/10.1016/j.sedgeo.2010.09.018
Tang RC, Jiang NQ, Liu SL (1983) Recognition of the geological setting and the seismogenic condition for the Diexi Magnitude 7.5 earthquake. J Seismol Res 6:327-338. (In Chinese)
Tanner PWG (1998) Interstratal dewatering origin for polygonal patterns of sand-filled cracks: a case study from late Proterozoic metasediments of Islay, Scotland. Sedimentology 45:71-89. https://doi.org/10.1046/j.1365-3091.1998.00135.xk
Topal S, Özkul M (2014) Soft-sediment deformation structures interpreted as seismites in the Kolankaya Formation, Denizli Basin (SW Turkey). Sci World J 2014:1-13. https://doi.org/10.1155/2014/352654
Törő B, Pratt BR (2015) Eocene paleoseismic record of the Green River Formation, Fossil Basin, Wyoming, U.S.A.: implications of synsedimentary deformation structures in lacustrine carbonate mudstones. J Sediment Res 85:855-884. https://doi.org/10.2110/jsr.2015.56
Törő B, Pratt BR (2016) Sedimentary record of seismic events in the Eocene Green River Formation and its implications for regional tectonics on lake evolution (Bridger Basin, Wyoming). Sediment Geol 344:175-204. https://doi.org/10.1016/j.sedgeo.2016.02.003
Üner S (2014) Seismogenic structures in Quaternary lacustrine deposits of Lake Van (eastern Turkey). Geologos 20:79-87. https://doi.org/10.2478/logos-2014-0011
Üner S (2018) Late Quaternary lacustrine storm deposits: sedimentological properties and regional significance (Lake Van Basin-Eastern Turkey). Arab J Geosci 11:1-12. https://doi.org/10.1007/s12517-018-3946-z
Üner S, Selçuk AS, Özsayın E (2019) Non-seismic soft-sediment

deformation structures from late Pleistocene lacustrine deposits of Lake Van (eastern Turkey): storm and overloading effect. J Great Lakes Res 45:664-671.https://doi.org/10.1016/j.jglr.2019.03.007
Valentine GA, Fierstein J, White JDL (2020) Soft sediment deformation in dry pyroclastic deposits at Ubehebe Crater, Death Valley, California. Geology 49:211-215. https://doi.org/10.1130/g48147.1
Wallace K, Eyles N (2015) Seismites within Ordovician–Silurian carbonates and clastics of southern Ontario, Canada and implications for intraplate seismicity. Sediment Geol 316:80-95. https://doi.org/10.1016/j.sedgeo.2014.12.004
Wang LS, Wang XQ, Shen JH, et al. (2020) Late Pleistocene environmental information on the Diexi paleo-dammed lake of the upper Minjiang River in the eastern margin of the Tibetan Plateau, China. J Mt Sci 17. https://doi.org/10.1007/s11629-019-5573-x
Wang LS, Wang XQ, Xu XN, et al. (2007) What happened on the upstream of Minjiang River in Sichuan Province 20,000 years ago. Earth Sci Front 14:189-196. (In Chinese)
Wang LS, Wang XQ, Xu XN, et al. (2012) Significances of studying the diexi paleo dammed lake at the upstream of minjiang river, sichuan, China. Quat Sci 32:998-1010. (In Chinese)
Wang LS, Yang LZ, Wang XQ, et al. (2005) Discovery of huge ancient dammed lake on upstream of Minjiang River in Sichuan , China. J Chengdu Univ Technol (Sci Technol Ed) 32:1-11. (In Chinese)
Wang MM, Lin AM (2017) Active thrusting of the Longquan Fault in the central Sichuan basin, China, and the seismotectonic behavior in the Longmen Shan fold-and-thrust belt. J Geophys Res Solid Earth 122:5639-5662. https://doi.org/10.1002/2016jb013391
Wang P, Zhang B, Qiu WL, et al. (2011) Soft-sediment deformation structures from the Diexi paleo-dammed lakes in the upper reaches of the Minjiang River, east Tibet. J Asian Earth Sci 40:865-872. https://doi.org/10.1016/j.jseaes.2010.04.006
Wang X (2009) The environment geological information in the sediments of Diexi ancient dammed lake on the upstream of Mingjiang River in Sichuan Province, China. PhD thesis, Chengdu University of Technology, Chengdu. p 116. (In Chinese)
Wang X, Li Y, Yuan Y, et al. (2014) Palaeoclimate and palaeoseismic events discovered in Diexi barrier lake on the Minjiang River, China. Nat Hazards Earth Syst Sci 14:2069-2078. https://doi.org/10.5194/nhess-14-2069-2014
Wang XG, Li CY, Lv LX, et al. (2017) Analysis of the late Quaternary activity along the Wenchuan-Maoxian fault-middle of the back-range fault at the Longmenshan Fault zone. Seismol Geol 39:572-586. (In Chinese)
Weaver JD, Jeffcoat RE (1978) Carbonate ball and pillow structures. Geol Mag 115. https://doi.org/10.1017/s0016756800037158
Wei Y, Wang X, Sheng M, et al. (2015) Reproduction of the sedimentary disturbance phenomenon of the Diexi ancient landslide-dammed lake under earthquake. J Mt Sci 12:1181-1188. https://doi.org/10.1007/s11629-015-3460-7
Wu LZ, Zhao DJ, Zhu JD, et al. (2019) A late Pleistocene river-damming landslide, Minjiang River, China. Landslides 17:433-444. https://doi.org/10.1007/s10346-019-01305-5
Xu H, Chen J, Cui ZJ, et al. (2020) Sedimentary facies and depositional processes of the Diexi ancient dammed lake, upper Minjiang River, China. Sediment Geol 398:1-15. https://doi.org/10.1016/j.sedgeo.2019.105583
Xu HY, Jiang H, Yu S, et al. (2015) OSL and pollen concentrate 14C dating of dammed lake sediments at Maoxian, east Tibet, and implications for two historical earthquakes in AD 638 and 952. Quat Int 371:290-299. https://doi.org/10.1016/j.quaint.2014.09.045
Yan JH, Chen SY, Jiang ZX, et al. (2007) Simulating experiment on genesis of seismo-turbidites in rift lacustrine basin. J Palaeogeogr 9:277-282. (In Chinese)
Yang WG (2005) Research of sedimentary record in terraces and climate vary in the upper reaches of Minjiang River, China. Master thesis, Chengdu University of Technology, Chengdu. p 75. (In Chinese)
Yang XP, Jiang P, Song FM, et al. (1999) The evidence of the south Longmenshan Fault zones cutting late Quaternary stratum. Seismol Geol 21:341-345. (In Chinese)
Yang YC, Li BY, Yin ZS, et al. (1982) The formation and evolution of landforms in the Xizang Plateau. Acta Geogr Sin 37:76-87. (In Chinese)
Youd TL (1975) Liquefaction, flow and associated ground failure. US Geological Survey Circular 688:1-12. https://doi.org/10.3133/CIR688
Zhang B, Wang P, Wang JC (2011) Discussion of the origin of the soft-sediment deformation structures in paleo-dammed lake sediments in the upper reaches of the Minjiang River. J Seismol Res 34:67-74. (In Chinese)
Zhang CH, Wu ZJ, Gao LZ, et al. (2007) Earthquake-induced soft-sediment deformation structures in the Mesoproterozoic Wumishan Formation, north China, and their geologic implications. Sci China Ser D 50:350-358. https://doi.org/10.1007/s11430-007-2038-9
Zhang JL, Ren JW, Chen CY, et al. (2013) Paleo-earthquake parameters of Minjiang Fault in Holocene. Earth Science-Journal of China University of Geosciences 38:83-90. (In Chinese)
Zhang SQ (2019) Characteristics and geological significance of the late Pleistocene lacustrine sediments in Diexi, Sichuan. Master thesis, China University of Geosciences, Beijing. p 76. (In Chinese)
Zhang YQ, Dong SW, Yang N (2009) Active faulting pattern, present-day tectonic stress field and block kinematics in the east Tibetan Plateau. Acta Geol Sin (Engl Ed) 83:694-712. https://doi.org/10.1111/j.1755-6724.2009.00093.x
Zhang YQ, Li J, Li HL, et al. (2016) Re-investigation on seismogenic structure of the 1933 Diexi Ms 7.5 earthquake, eastern margin of the Xizang (Tibetan) Plateau. Geol Rev 62:267-276. (In Chinese)
Zhang YQ, Li HL (2010) Late Quaternary active faulting along the SW segment of the Longmenshan Fault zone. Quat Sci 30. (In Chinese)
Zhao QH, Zheng XH, He WX, et al. (2023) Determination of Songpinggou Fault in Diexi, Sichuan. J Eng Geol 31:1964-1974. (In Chinese)
Zhao SY, Chigira M, Wu XY (2019) Gigantic rockslides induced by fluvial incision in the Diexi area along the eastern margin of the Tibetan Plateau. Geomorphology 338:27-42. https://doi.org/10.1016/j.geomorph.2019.04.008
Zheng LJ, Jiang ZX, Liu H, et al. (2015) Core evidence of paleoseismic events in Paleogene deposits of the Shulu Sag in the Bohai Bay Basin, east China, and their petroleum geologic significance. Sediment Geol 328:33-54. https://doi.org/10.1016/j.sedgeo.2015.07.013
Zhong JH, Ni LT, Hao B, et al. (2017) Discovery of large-scale dish-like structures of the Lower Cretaceous in Ordos Basin and its geological significance. J Palaeogeogr 19:73-88. (In Chinese)
Zhong N (2017) Earthquake and provenance analysis of the lacustrine sediments in the upper reaches of the Min River during the late Pleistocene. PhD thesis, China Earthquake Administration, Beijing. p 193. (In Chinese)
Zhong N, Bai YL, Xu HY, et al. (2024) A continuous 18.6-10 ka record of seismic events revealed by Xinmocun lacustrine sediments at Diexi, eastern Tibetan Plateau. J Asian Earth Sci 267:1-16. https://doi.org/10.1016/j.jseaes.2024.106152
Zhong N, Jiang HC, Li H, et al. (2019) Last Deglacial Soft-Sediment Deformation at Shawan on the Eastern Tibetan Plateau and Implications for Deformation Processes and Seismic Magnitudes. Acta Geol Sin (Engl Ed) 93:430-450. https://doi.org/10.1111/1755-6724.13773
Zhong N, Jiang HC, Li HB, et al. (2022) The potential of using soft-sediment deformation structures for quantitatively reconstructing paleo-seismic shaking intensity: progress and prospect. Environ Earth Sci 81. https://doi.org/10.1007/s12665-022-10504-8
Zhong N, Jiang HC, Li HB, et al. (2023) A continuous 18-10.2 ka paleo-earthquake events revealed by the Luobozhai lacustrine sediments, eastern Tibetan Plateau. Quat Int 673:40-52. https://doi.org/10.1016/j.quaint.2023.10.003
Zhou RJ, Li Y, Alexander LD, et al. (2006) Active tectonics of the eastern margin of the Tibet Plateau. Mineral Petrol 26:40-51. (In Chinese)